Quaternary Science Advances 4 (2021) 100037

Contents lists available at ScienceDirect

Quaternary Science Advances

journal homepage: www.sciencedirect.com/journal/quaternary-science-advances

Quantitative impact of astronomical and sun-related cycles on the Pleistocene climate system from Antarctica records

Paolo Viaggi

Museo Geologico Giovanni Capellini, Bologna University, Via Zamboni 63, I-40126, Bologna, Italy

ARTICLE INFO

Keywords:
Quantitative impact
Planetary beat hypothesis
Singular spectrum analysis
Solar cycles
Heinrich-bond
Hallstatt

ABSTRACT

We use the benefits of the full-resolution methodology for time-series decomposition singular spectrum analysis to assess the quantitative impact of orbital and, for the first time, millennial-scale Sun-related climate responses from EPICA records. The quantitative impact of the three Sun-related cycles (unnamed ~9.7-kyr; proposed 'Heinrich-Bond' ~6.0-kyr; Hallstatt ~2.5-kyr), cumulatively explain ~4.0% (δD), 2.9% (CO_2), and 6.6% (CH_4) in variance, demonstrating for the first time the minor role of solar activity in the regional budget of Earth's climate forcing. A cycle of ~3.6 kyr, which is little known in literature, results in a mean variance of 0.6% only, does not seem to be Sun-related, although a gravitational origin cannot be ruled out. According to the recurrence analysis of Heinrich events (6.03 ± 1.4 kyr) and their correlation with EPICA stack ~6.0-kyr cycle, it is proposed that this band of solar activity be named the 'Heinrich-Bond cycle'. On these basis, it is deemed that the 'Heinrich-Bond' solar cycle may act on the ice-sheet as an external instability factor both related to excess ice leading to calving process and IRD-layers ('cold-related' Heinrich events), and surface heating with meltwater streams ('warm-related' Heinrich events). The Hallstatt cycle is found in a number of solar proxies, geomagnetic secular variations, paleoclimatic oscillations, combination tones of Milankovitch forcings and resonant planetary beats, indicating an apparent 'multi-forcing' origin possibly related to planetary beat hypothesis. The orbital components consistently reflects the post-Mid-Pleistocene transition nature of the EPICA records in which the short eccentricity results in most of the variance (51.6%), followed by obliquity (19.0%) and precession (8.4%). Beyond the Milankovitch theory, evidence is emerging of a multiple-forcing cosmoclimatic system with stochastic interactions between external (gravitational resonances, orbitals, solar activity) and Earth's internal (geodynamics, atmosphere composition, feedback mechanisms) climate components, each having a strong difference in terms of the relative quantitative impact on Earth's climate.

1. Introduction

In recent years, several attempts have been made to reconstruct high-resolution paleoclimatic 'reference' sections, such as the Pliocene-Pleistocene record of the global ice volume and deep-ocean temperature (LR04 benthic $\delta^{18}O$ stack; Lisiecki and Raymo, 2005) or the Pleistocene 800,000 years-long time series of atmospheric greenhouse gas (GHG) concentration (CO_2, CH_4) and temperature proxy (δD) from the European Project for Ice Coring in Antarctica (EPICA) (Luthi et al., 2008; Loulergue et al., 2008; Bereiter et al., 2015; Past interglacials working group of PAGES, 2016). These records provide a common framework and a good opportunity to study different aspects of the Plio-Pleistocene climate system. This research applies advanced signal decomposition procedure to the Pleistocene ice-core records of EPICA Past Interglacials Working Group (Past interglacials working group of PAGES, 2016) to estimate the quantitative impact of climate components. The aim of the present study is to investigate the changes of the Pleistocene climate over the last 800 kyr (thousand years) of EPICA temperature and GHG records by using the benefits of the full-resolution methodology for time-series decomposition singular spectrum analysis (SSA) (Elsner and Tsonis, 1996), with a special focus on Sun-related signals. In fact, owing to the high resolution and the relatively homogeneous sample interval of the δD, CO_2, and CH_4 records, the methodology allowed these signals to be decomposed from orbital up to sub-Milankovitch frequency bands (2.5-kyr Hallstatt cycle), providing a more complete picture of these new Antarctic high frequency signals. These 800-kyr-long suborbital records, which include some possible Sun-related signals, fill an important gap in the field of solar cycles offering for the first time an estimate of their quantitative impact on the Pleistocene climate system and their presumed correlation with the glaciological events of North Atlantic and

E-mail address: paolov6363@yahoo.it.

https://doi.org/10.1016/j.qsa.2021.100037
Received 1 March 2021; Received in revised form 21 June 2021; Accepted 28 June 2021
Available online 1 July 2021

Greenland (Channell et al., 2012; Rasmussen et al., 2014). The Sun is the main source of energy for the Earth's climate system through two main variations in solar radiation: changes in the Earth's orbit around the Sun over several tens and hundreds of thousands of years, which affect the amount and distribution of radiant energy hitting the Earth (astronomical forcing) (Berger, 1988; Imbrie et al., 1992; Pillans et al., 1998; Laskar et al., 2011); second, internal stellar processes over several tens and thousands of years affect the total radiant energy emitted by the Sun - i.e. solar activity (SA; solar forcing) (Clemens, 2005; Haigh 2011; Vieira et al., 2011; McCracken et al., 2014; Zhao and Feng, 2015; Usoskin, 2017; Zharkova et al., 2019). The Earth's climate can be understood as the balance between the energy input from the Sun and the energy dispersed into space through the action of the Earth's atmospheric GHGs and internal feedback processes of the climate system. However, the degree to which SA has affected the Earth's climate in the past and in the present owing to recent climate change is still a matter of debate, especially with regard to future developments in solar activity which might either moderate or amplify the climate change (Svensmark and Friis-Christensen, 1997; Neff et al., 2001; Sun and Bradley, 2002; Ogurtsov et al., 2002; Bard and Frank, 2006; Gray et al., 2010; Vieira et al., 2011; Engels and van Geel, 2012; Mörner et al., 2013b; Wu et al., 2018b; Shindell et al., 2020). Several reasons for this long debate include the relatively short length of continuous data of direct or proxy observations in SA (Zhao and Feng, 2015), the low resolution of some climate records, together with traditional methods of spectral analysis sometimes little resolutive in discriminating high frequency cycles, and with a non-implicit approach to the quantitative estimation of signal variance (Kominz and Pisias, 1979; Wunsch, 2004; Viaggi, 2018).

2. Materials and methods

The EPICA δD, CO_2, and CH_4 records (Jouzel et al., 2007; Luthi et al., 2008; Loulergue et al., 2008; Bereiter et al., 2015; Past interglacials working group of PAGES, 2016) were considered as materials for signal processing. The time-series provided by Past interglacials working group of PAGES (2016) were chosen because they are recalibrated on the AICC2012 age model (Bazin et al., 2013) and the CO_2 oldest EPICA Dome C section was published by Luthi et al. (2008) and Siegenthaler et al. (2005), which was subsequently updated by Bereiter et al. (2015). Therefore, the differences in the age model between the EPICA records should be negligible. The AICC2012 age model has been constructed combining glaciological inputs and data constraints, including a wide range of relative and absolute gas and ice stratigraphic markers. The uncertainty of AICC2012 is ± 2.6 kyr on average during the past 100–720 kyr (Bazin et al., 2013). The δD, CO_2, and CH_4 records provided by Past interglacials working group of PAGES (2016) exhibit a mean data-spacing of 1.00 ± 0.06 kyr, 0.83 ± 0.48 kyr, and 1.05 ± 0.24 kyr, respectively. The δD proxy depends on Antarctic site temperatures derived from the ratios of water isotopes in ice cores (Jouzel et al., 1997). CO_2 and CH_4 concentrations can be determined directly from measurements in the air within ice cores (Luthi et al., 2008; Loulergue et al., 2008). The CH_4 content results from changes in wetlands in the tropics and high northern latitudes (Loulergue et al., 2008; Past interglacials working group of PAGES, 2016). Thus, ice core CH_4 may be viewed as a signal integrating parts of the northern hemisphere terrestrial biosphere (Loulergue et al., 2008; Luthi et al., 2008; Past interglacials working group of PAGES, 2016). The NGRIP $\delta^{18}O$ data on GICC05 age model (NGRIP Community Members, 2007) were used to correlate the glaciological events of the North Atlantic and Greenland regions.

The δD, CO_2, and CH_4 records were partitioned in signal components using singular spectrum analysis. The SSA is an advanced method for time-series analysis used to isolate full-resolution independent signal components based on the signal strength (variance) (Vautard and Ghil, 1989; Elsner and Tsonis, 1996; Ghil et al., 2002; Hassani, 2007; Viaggi, 2018). In contrast with Fourier analysis with a fixed basis of sine and cosine functions, SSA uses an adaptive basis generated by the time series itself. As a result, the underlying model in SSA is more general and can extract amplitude-modulated wave components with higher resolution than Fourier analysis. Indeed, the most important feature of the SSA is the high-resolution separation of signal components containing little power (according to Nyquist's condition), together with an implicit approach towards the quantitative estimation of the signal strength by variance, which is a fundamental task in paleoclimatology. SSA can be effectively applied as a non-parametric method for the detection of structural changes in the time series, reflecting the main physical phenomena underlying the data (Vautard and Ghil, 1989; Hassani, 2007). SSA requires evenly spaced records. The δD, CO_2, and CH_4 records were resampled at constant time intervals of 0.5 kyr by robust cubic spline interpolation algorithm which prevents artifacts generation. The SSA enabled each of the resampled signals to be decomposed into nine-component time-series without overcoming the resolution limits of the original data, according to Nyquist's condition (δD~2.0 kyr; CO_2 ~1.7 kyr; CH_4 ~2.1 kyr) (see Additional file 1, section 2). Consequently, the highest frequency identified in the present work is in the ~2.5-kyr band with a good quality signal, statistically significant and highly coherent with the filtered Hallstatt component from the total solar irradiance (TSI) proxy of Steinhilber et al. (2012) (Additional file 1, section 4). The slight oversampling at 0.5-kyr is functional in preserving this last cycle by cubic spline interpolation which did not generate any frequency artifacts (Additional file 1, Table S3). In fact, the high frequency cycles here identified by SSA are natural and statistically significant components of the original records. The SSA is achieved by the computation of forward-backward covariance matrices with a 60-order (embedding dimension) using the singular-value decomposition procedure. A nested-SSA approach has been applied to some high-variance components to better separate some frequency bands and to correctly estimate the variance fraction, and this is done by increasing the embedding dimension up to 255 and partitioning the component into subcomponents (Viaggi, 2018). More details on parameter selection criteria can be found in Additional file 1. A very small residual variance still superimposed to some subcomponents has been resolved by Wavelet and Savitzky-Golay filtering algorithms. Wavelet filtering with complex Morlet continuous wavelet transform and adjustable parameter of 8, was used to isolate the obliquity modulation cycle (~160–240 kyr) with the frequency range 0.0035–0.007 kyr^{-1}, while Savitzky-Golay filter is particularly useful for highlighting weak trends and therefore was applied to isolate the mid-term oscillation. The Savitzky-Golay filter used is a 4-order least squares polynomial fitting across a moving window of 400. The variance strength of the δD, CO_2, and CH_4 reconstructed records by forcing is computed as the sum of the absolute variance of the related components and subcomponents identified, and their signals are calculated as a weighted mean by variance. The EPICA stack by forcing is calculated as weighted mean by variance of the standardized δD, CO_2, and CH_4 signals (detailed explanations in Additional file 1). The SSA-components are then investigated by Fourier frequency spectrum (FFS) with data window to analyse the frequency power and test for component significance by first-order autoregressive AR(1) process. The data tapering used in this study is the cs2-Hann window and the Prime Factor fast Fourier transform algorithm. The peak detection uses peak-based critical limit significance levels. For this type of robust confidence limit, one seeks to disprove the null hypothesis, where one postulates either a red or white noise background. Unless otherwise indicated, the frequency peaks shown in this study are the most significant peaks above a 99.9% critical limit. Thus, the high frequency cycles discussed in the text are natural and statistically significant components related to tangible physical processes. For each peak, the time-integral squared amplitude (TISA) power is computed as a relative percentage. The summed power reported in the frequency analysis is merely the sum of the component powers, and not the power of the composite signal that would result from the addition of the components. Finally, the phase relationships of the δD vs. CO_2 and CH_4 standardized (mean = 0;

standard deviation = 1) components were examined by cross-spectral analysis with Hann window. In the present study, additional investigations (FFS, long-term smoothing by Savitzky-Golay filter and cross-spectral analysis) were performed on three recent Holocene solar proxies (Vieira et al., 2011; Steinhilber et al., 2012; Wu et al., 2018a) to further support the discussion on the EPICA millennial-scale Sun-related cycles. The Savitzky-Golay filter used in solar proxies is a 4-order least squares polynomial fitting across a moving window of 100 (Steinhilber et al., 2012), 200 (Vieira et al., 2011) and 250 (Wu et al., 2018a). In particular, Steinhilber et al. (2012) combined different ^{10}Be ice core records obtained from Greenland and Antarctica with the global ^{14}C tree ring record using principal component analysis, and the new cosmic radiation record was then used to reconstruct a TSI signal which minimized the Earth's system effects influencing the radionuclide signal (e.g. climate-induced transport and deposition changes, changes in the carbon cycle) (Mayewski et al., 1997; Solanki et al., 2004; Steinhilber et al., 2012; Charvátová and Hejda, 2014; Usoskin, 2017). Thus, this TSI record is considered by the authors as a valuable proxy of the SA, and was used in cross-spectral analysis to support the interpretation of the Hallstatt cycle. Further details on the applied methodology in this study and a discussion of the quality and reliability of the time series processing can be found in Additional file 1. The dataset of the EPICA SSA-components and stacks can be found in Additional file 2. The software used in this research is AutoSignal™.

3. Results and discussion

3.1. Signals decomposition and interpretation

Nine SSA components (abbreviated as comp) were identified from each δD, CO_2 and CH_4 records spanning from mid-term oscillation to astronomical and suborbital signals. The first three components were processed into subcomponents (abbreviated as subcomp) to better separate some oscillatory terms. A detailed description of extracted components and subcomponents can be found in Additional file 1. From an interpretative perspective, the sub-Milankovitch comp-5-6s, -7-8s, -9-15s, -16-23s, and -24-26s are discussed in the dedicated section 3.2 with a special focus on the Sun-related signals. Next, the main features of the SSA-components are described by records in descending order of periodicity.

3.1.1. EPICA δD

The δD SSA-components cumulatively explain 99.95% of the original variance (δD filtered). The spectral analysis of these δD components ranged from 159 kyr to 2.4 kyr periodicity (Fig. 1, Table 1).

δD component-1: This component explains 46.9% of the total variance without any evident signal trend. The FFS shows a dominant 93-kyr short eccentricity cycle (TISA power 79.9%) with an ancillary term of 159 kyr close to the obliquity modulation cycles (~160–200 kyr) (Boulila et al., 2011; Viaggi, 2018) and a low significance obliquity signal. The subcomponents analysis (see Additional file 1) reveals a weak mid-term oscillation (not detected by FFS) from which a variance of 2.0% may be estimated, along with a 3.7% variance of the obliquity modulation cycle. The mid-term oscillation shows a mild warming phase centred at ~400 kyr, and correlates to the wide swing of LR04 δ^{18}O depletion that peaks at approximately 400–300 kyr, which is referred to as the Mid-Brunhes Oscillation (MBO) (Viaggi, 2018), and containing the Mid-Brunhes Event at approximately 430 kyr (Berger and Yin, 2012). Note that the MBO is not related to the long eccentricity band (~400-kyr) because 400 kyr ago this cycle was on a minimum (Laskar et al., 2011).

δD component-2: Component-2 explains 30.8% of the total variance and exhibits a 41-kyr obliquity cycle (power 52.8%) envelopes in a 92 kyr (26.5%) and 75 kyr (20.7%) short eccentricity framework (Fig. 1). This feature is similar to that shown by global δ^{18}O and equatorial Site 846 sea surface temperature (SST) components-3-4 after the Mid-Pleistocene transition (MPT), showing the envelope of two to three obliquity cycles in a weak eccentricity 93-kyr framework (Fig. 4 and Fig. 8 in Viaggi, 2018).

δD component-3: This signal explains 10.1% in the variance modulated by a 23-kyr precession cycle (power 54.7%) within an obliquity framework of 41 kyr (25.7%) and 31 kyr (19.6%).

δD component-4: This is a 4.2% variance 21-kyr precession component.

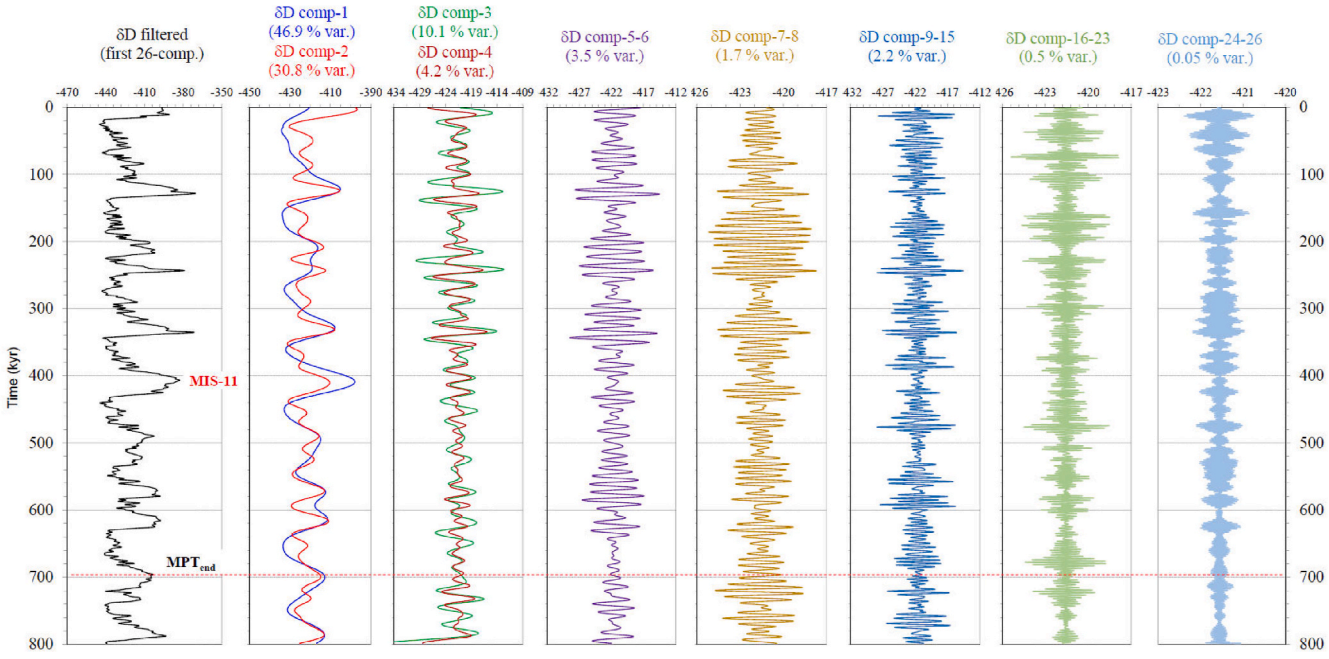

Fig. 1. Time-series panel of the nine δD components isolated from the EPICA record by singular spectrum analysis, together with the δD-filtered record (left) obtained by combining these data components (99.95% total variance). See Table 1 for Fourier frequency results and forcing interpretation. The x-axis scale (‰) is variable in relation to the variance fraction of the data components (in brackets). EPICA original data from Past interglacials working group of PAGES (2016). Time scale in kyr.

Table 1
Quantitative estimation of signal magnitude (percentage variance) and Fourier frequency results of the nine EPICA δD components isolated by singular spectrum analysis. Interpretation of the suborbital forcings in the section "New Evidence of Solar Cycles from EPICA records". Unless otherwise indicated, the frequency peaks are the most significant peaks above a 99.9% critical limit. EPICA original data from Past interglacials working group of PAGES (2016).

δD component rank	δD component variance	Frequency (kyr^{-1})	TISA power (%)	Period (kyr)	Weighted mean period (kyr)	Forcing
1	46.9%	0.01071420	79.9	93		Short eccentricity (with obliquity modulation cycle)
		0.00628129	17.6	159		
		0.02460160	2.5	41	low significance	
2	30.8%	0.02458230	52.8	41		Obliquity with short eccentricity envelopes
		0.01090870	26.5	92		
		0.01341453	20.7	75		
3	10.1%	0.04262501	54.7	23		Precession and obliquity
		0.02455350	25.7	41		
		0.03261513	19.6	31		
4	4.2%	0.04274945	59.6	23	21	Precession
		0.05841370	31.1	17		
		0.05460236	9.3	18		
5–6	3.5%	0.08695223	44.5	11.5	13	Half-precession
		0.08281695	32.0	12.1		
		0.06577397	23.6	15.2		
7–8	1.7%	0.09781210	36.0	10.2	9.2	Sun
		0.11021661	34.7	9.1		
		0.12489587	29.3	8.0		
9–15	2.2%	0.15272879	36.3	6.5	5.7	Sun
		0.17509093	31.9	5.7		
		0.21732064	31.8	4.6		
16–23	0.5%	0.30638180	43.8	3.3	3.4	Unclear
		0.27912013	28.7	3.6		
		0.29903889	27.5	3.3		
24–26	0.05%	0.43138037	47.2	2.3	2.4	Sun
		0.43613177	31.2	2.3		
		0.37534885	21.6	2.7		
>26	0.05%					Noise

δD component-5-6: This component of the 3.5% variance is paced by the 13-kyr cycle, which is related to the half-precession band of equatorial origin modulated at 11–12 kyr (Hagelberg et al., 1994; Berger et al., 2006; Sun and Huang, 2006; Viaggi, 2018).

δD component-7-8: Component-7-8 incorporates 1.7% of the δD variance at the 9.2-kyr periodicity band.

δD component-9-15: This explains the 2.2% variance in the frequency band at 5.7 kyr.

δD component-16-23: A 3.4 kyr period is shown by this component, explaining 0.5% of the δD variance.

δD component-24-26: this last component includes 0.05% of the signal variance, and shows an oscillatory beat at 2.4 kyr.

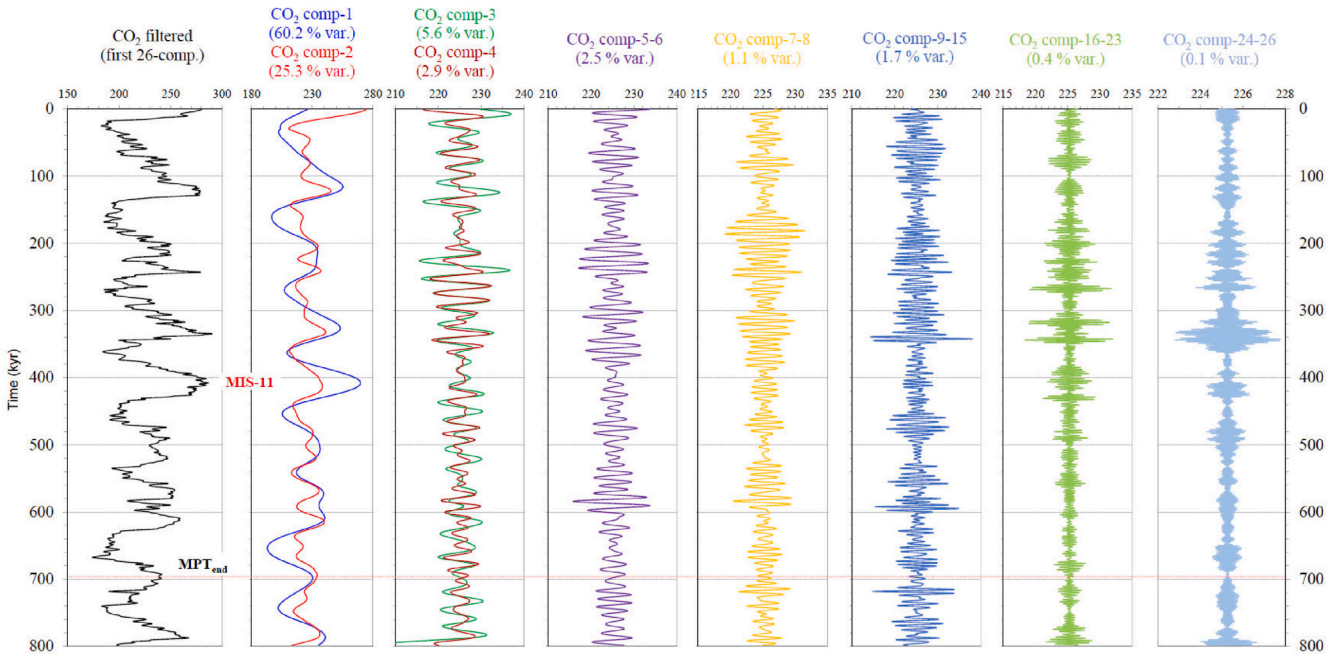

Fig. 2. Time-series panel of the nine CO_2 components isolated from the EPICA record by singular spectrum analysis, together with the CO_2-filtered record (left) obtained by combining these data components (99.8% total variance). See Table 2 for Fourier frequency results and forcing interpretation. The x-axis scale (ppm) is variable in relation to the variance fraction of the data components (in brackets). EPICA original data from Past interglacials working group of PAGES (2016). Time scale in kyr.

3.1.2. EPICA CO_2

The CO_2 SSA-components cumulatively explain 99.8% of the original variance (CO_2 filtered). The spectral framework of these CO_2 components ranges from 239 kyr to 2.5 kyr periodicity (Fig. 2; Table 2).

CO_2 component-1: This explains 60.2% of the variance with any evidence of signal trend. The FFS shows a dominant 96-kyr short eccentricity cycle (power 72.5%) with an ancillary term of 239 kyr (26.6%), which may be related to the obliquity modulation cycles (~160–200 kyr). The subcomponents analysis exhibits a mid-term oscillation (not detected by FFS) similar to that of the δD component-1, from which a variance of 7.7% may be estimated, along with a 5.8% variance related to the obliquity modulation cycle.

CO_2 component-2: This component explains 25.3% of the variance in the 46-kyr obliquity (power 23.4%) and 95–76-kyr short eccentricity bands (50.0% and 26.6%, respectively), with similar features as the δD component-2 (Fig. 2).

CO_2 component-3: This explains the variance of 5.6%, which results from a 23-kyr precession cycle (power 73.7%) with obliquity envelopes at 41 kyr and 31 kyr.

CO_2 component-4: This component constitutes 2.9% of the EPICA CO_2 variance and exhibits a weight mean period at the 21-kyr precession band.

CO_2 component-5-6: This high-frequency component explains 2.5% of the variance paced by the 13-kyr band related to the half-precession cycle.

CO_2 component-7-8: Component-7-8 incorporates 1.1% of the CO_2 variance at the 9.8-kyr weighted mean periodicity.

CO_2 component-9-15: this signal explains 1.7% of the variance, and exhibits a weighted mean periodicity of 5.9 kyr.

CO_2 component-16-23: A 3.6-kyr cycle is shown by this component, explaining 0.4% of the CO_2 variance.

CO_2 component-24-26: this last component has a signal variance of only 0.1%, and exhibits an oscillatory beat at 2.5 kyr.

3.1.3. EPICA CH_4

The CH_4 SSA-components are responsible for 99.6% of the signal variance (CH_4 filtered), with oscillations ranging from 165 kyr to 2.5 kyr periodicity (Fig. 3, Table 3).

CH_4 component-1: component-1 describes 44.7% of the total variance, and shows a dominant 96-kyr short eccentricity cycle (power 83.5%) with an auxiliary term of 165 kyr (14.3%) relative to the obliquity modulation cycle. The analysis of the subcomponents shows a mid-term oscillation (not detected by FFS) similar to that of the previous ones, from which a variance of 3.5% may be estimated, along with a 2.5% variance related to the obliquity modulation cycle.

CH_4 component-2: This signal explains 27.5% of the variance in the 41-kyr obliquity (power 47.5%) and 96-75-kyr short eccentricity bands (30.7% and 21.8%, respectively). The CH_4 component-2 has similar features as the CO_2 component-2 (Fig. 3).

CH_4 component-3: This shows a total variance of 9.3% resulting from a 22-kyr precession cycle (42.0%) with obliquity envelopes at 41 kyr and 29 kyr.

CH_4 component-4: This component explains a variance of 5.2% resulting from a mean precession period of ~20 kyr.

CH_4 component-5-6: The high-frequency component-5-6 exhibits 5.3% of the variance with a weighted mean periodicity of ~13 kyr relative to the half-precession cycle.

CH_4 component-7-8: This signal contains a frequency beat at 9.0 kyr with a 2.6% variance covering.

CH_4 component-9-15: This component exhibits 3.8% of the variance and exhibits a mean periodicity at about 5.4 kyr.

CH_4 component-16-23: A 1.0% variance in the 3.6-kyr frequency band characterizes component-16-23.

CH_4 component-24-26: This results in a signal variance of 0.2% with a 2.5-kyr periodicity.

Table 2
Quantitative estimation of signal magnitude (percentage variance) and Fourier frequency results of the nine EPICA CO_2 components isolated by singular spectrum analysis. Interpretation of the suborbital forcings in the section "New Evidence of Solar Cycles from EPICA records". Unless otherwise indicated, the frequency peaks are the most significant peaks above a 99.9% critical limit. EPICA original data from Past interglacials working group of PAGES (2016).

CO_2 component rank	CO_2 component variance	Frequency (kyr^{-1})	TISA power (%)	Period (kyr)	Weighted mean period (kyr)	Forcing
1	60.2%	0.01046401	72.5	96		Short eccentricity (with obliquity modulation cycle)
		0.00419271	26.6	239		
		0.01790364	0.9	56	low significance	
2	25.3%	0.02162145	23.4	46		Obliquity with short eccentricity envelopes
		0.01050971	50.0	95		
		0.01324018	26.6	76		
3	5.6%	0.04270651	73.7	23		Precession and obliquity
		0.03216239	15.7	31		
		0.02450036	10.6	41		
4	2.9%	0.04276472	58.0	23	21	Precession
		0.05834638	36.6	17		
		0.06172018	5.3	16		
5–6	2.5%	0.06632120	26.5	15.1	13	Half-precession
		0.07404669	25.3	13.5		
		0.08001619	48.1	12.5		
7–8	1.1%	0.09520119	27.1	10.5	9.8	Sun
		0.09805263	36.9	10.2		
		0.11222552	36.0	8.9		
9–15	1.7%	0.15264722	34.9	6.6	5.9	Sun
		0.16891074	28.1	5.9		
		0.19058835	37.0	5.2		
16–23	0.4%	0.25642887	41.8	3.9	3.6	Unclear
		0.27835945	29.0	3.6		
		0.31717431	29.2	3.2		
24–26	0.1%	0.39283997	44.6	2.5	2.5	Sun
		0.39637938	28.5	2.5		
		0.39937111	26.9	2.5		
>26	0.2%					Noise

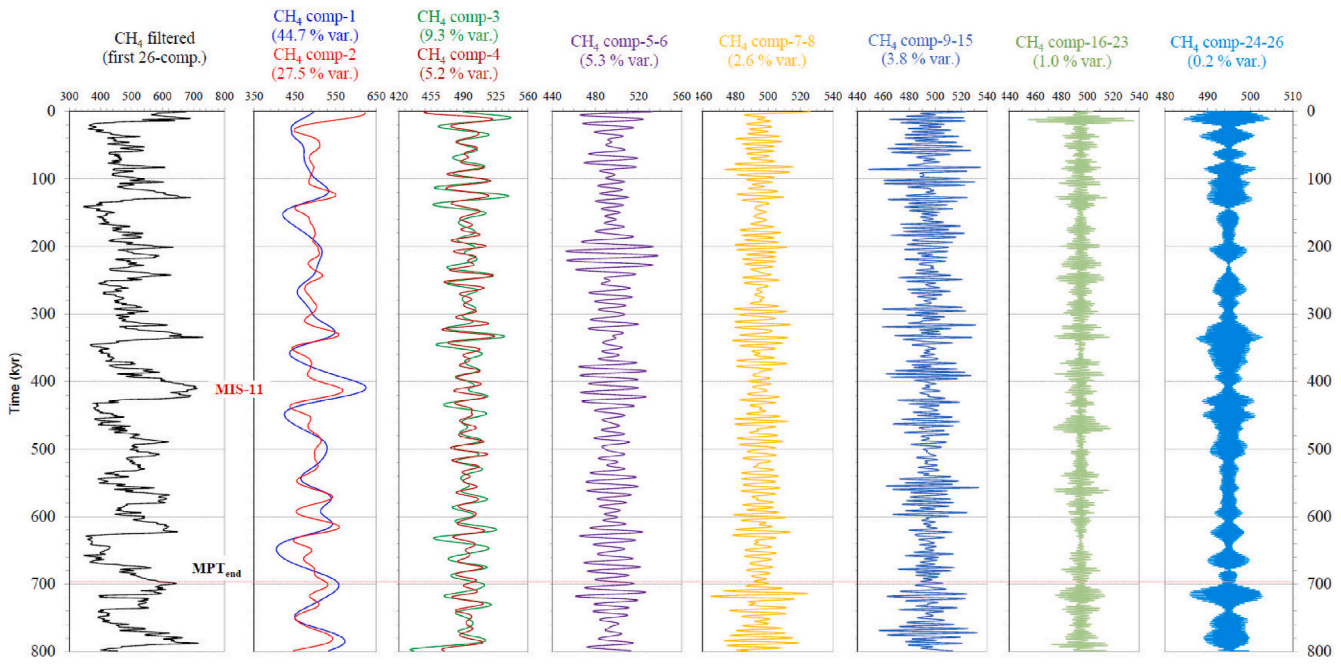

Fig. 3. Time-series panel of the nine CH_4 components isolated from the EPICA record by singular spectrum analysis, together with the CH_4-filtered record (left) obtained by combining these data components (99.6% total variance). See Table 3 for Fourier frequency results and forcing interpretation. The x-axis scale (ppb) is variable in relation to the variance fraction of the data components (in brackets). EPICA original data from Past interglacials working group of PAGES (2016). Time scale in kyr.

3.2. *New evidence of solar cycles from EPICA records*

The SSA processing has enabled the δD, CO_2, and CH_4 records (abbreviated as DCM) to be split into new statistically significant sub-Milankovitch 800,000-yr long time-series, ranked for the first time by signal strength and discussed in this section (DCM comp-5-6s, -7-8s, -9-15s, -16-23s, -24-26s). The sub-Milankovitch bands (1-15-kyr periodicity) are millennial-scale oscillations that occur over a wide spectrum of paleoceanographic, paleogeographic, paleoclimatic and paleoenvironmental conditions for time periods spanning from Cambrian to the Quaternary (Elrick and Hinnov 2007). Although extensively studied, no conclusive hypothesis explains their origin, even though recent studies on multi-millennial solar proxies and solar magnetic fields imply a Sun-related origin for some suborbital bands (Table 4). The occurrence of these quasi-periodic climate changes is interpreted as being related to internal mechanisms, such as ice sheet dynamics or ocean-atmosphere system variations (MacAyeal, 1993; Alley et al., 1999), or to external mechanisms, including (1) the biannual passage of the Sun across the intertropical zone induces hemi-precession (~12 kyr) cycles (Berger et al., 2006; Sun and Huang, 2006); (2) nonlinear signal transformation produces suborbital harmonics or combination tones of primary Milankovitch cycles (Pestiaux et al., 1988; Rodrìguez-Tovar and Pardo-Igùzquiza, 2003; Franco and Hinnov 2012; Franco et al., 2012; Da Silva et al., 2018) and (3) solar forcing (Dergachev, 2004; Elrick and Hinnov 2007; Xapsos and Burke, 2009; Vieira et al., 2011; Steinhilber et al., 2012; McCracken et al., 2014; Usoskin et al., 2016; Usoskin, 2017). A debated planetary beat hypothesis (PBH) on SA (Charvátová, 2000; Abreu et al., 2012; Scafetta 2012, 2014a; Mörner, 2013; Mörner et al., 2013a; Holm, 2014; Cauquoin et al., 2014; McCracken et al., 2014; Yndestad and Solheim, 2016; Sánchez-Sesma, 2016; Scafetta et al., 2016; Zharkova et al., 2019) could reconcile the apparent contradiction of suborbital cycles with similar quasi-periods across solar proxies and nonlinear harmonics and/or combination tones of primary Milankovitch cycles (Table 4). In fact, according to PBH, the motion of the giant planets generates a beat on the Sun in the form of gravity (tidal force) and angular momentum with respect to the solar system's barycenter, which is called solar inertial motion (SIM) (Charvátová, 2000; Paluš et al., 2007; McCracken et al., 2014; Scafetta et al., 2016; Zharkova et al., 2019). The planetary beat may thus affect the Earth both directly via its gravity pulse, as well as indirectly via its effects on the solar dynamo, acting the solar wind control on the incoming cosmic rays, and thus also on the production of cosmogenic radionuclides (Charvátová, 2000; Paluš et al., 2007; Abreu et al., 2012; Mörner et al., 2013b; McCracken et al., 2014; Zharkova et al., 2019), although the physical problem remains unclear (McCracken et al., 2014; Scafetta, 2014b).

Indeed, none of the known solar cycles (11–22, 60–65, 80–90, 110–140, 160–240, ~500 and 800–1200 year bands) can be explained using current physical models based on mainstream solar theories, and this may be because solar dynamics is not determined by internal solar mechanisms alone (Scafetta, 2012). Another possible reason is that the physics explaining the dynamical evolution of the Sun is still largely unknown (Scafetta, 2012). Recently discovered long-term oscillations of the solar background magnetic field associated with double dynamo waves generated in inner and outer layers of the Sun were found to be related to the long-term SIM of the solar system, and are closely linked to total solar irradiance (Zharkova et al., 2019). Thus, the solar system can be considered as a resonator of planetary orbital periods characterized by a specific harmonic planetary structure that also synchronizes the Sun's activity and the Earth's climate (McCracken et al., 2014; Scafetta, 2014a; Scafetta et al., 2016). The SA – i.e. the emission of heat, electromagnetic waves, and particles – is known to change with cycles ranging from several years to decades, centuries, and millennia (Kern et al., 2012; Mörner et al., 2013b; Usoskin, 2017; Wu et al., 2018a). Direct satellite measurements or historical observations can be used to study short-term solar cyclicity, such as the 11-year Schwabe cycles (also known as sunspot-cycle) and the Gleissberg cycle, which have a characteristic double periodicity of 50–80 years and 90–140 years, respectively (Ogurtsov et al., 2002; Kern et al., 2012; Scafetta, 2012). Proxy data are necessary to test much longer periodicities. Cosmic-ray produced radionuclides, such as ^{14}C and ^{10}Be, which are stored in tree rings and polar ice cores, offer the opportunity to reconstruct the history of cosmic radiation and SA over millennia by removing the Earth's

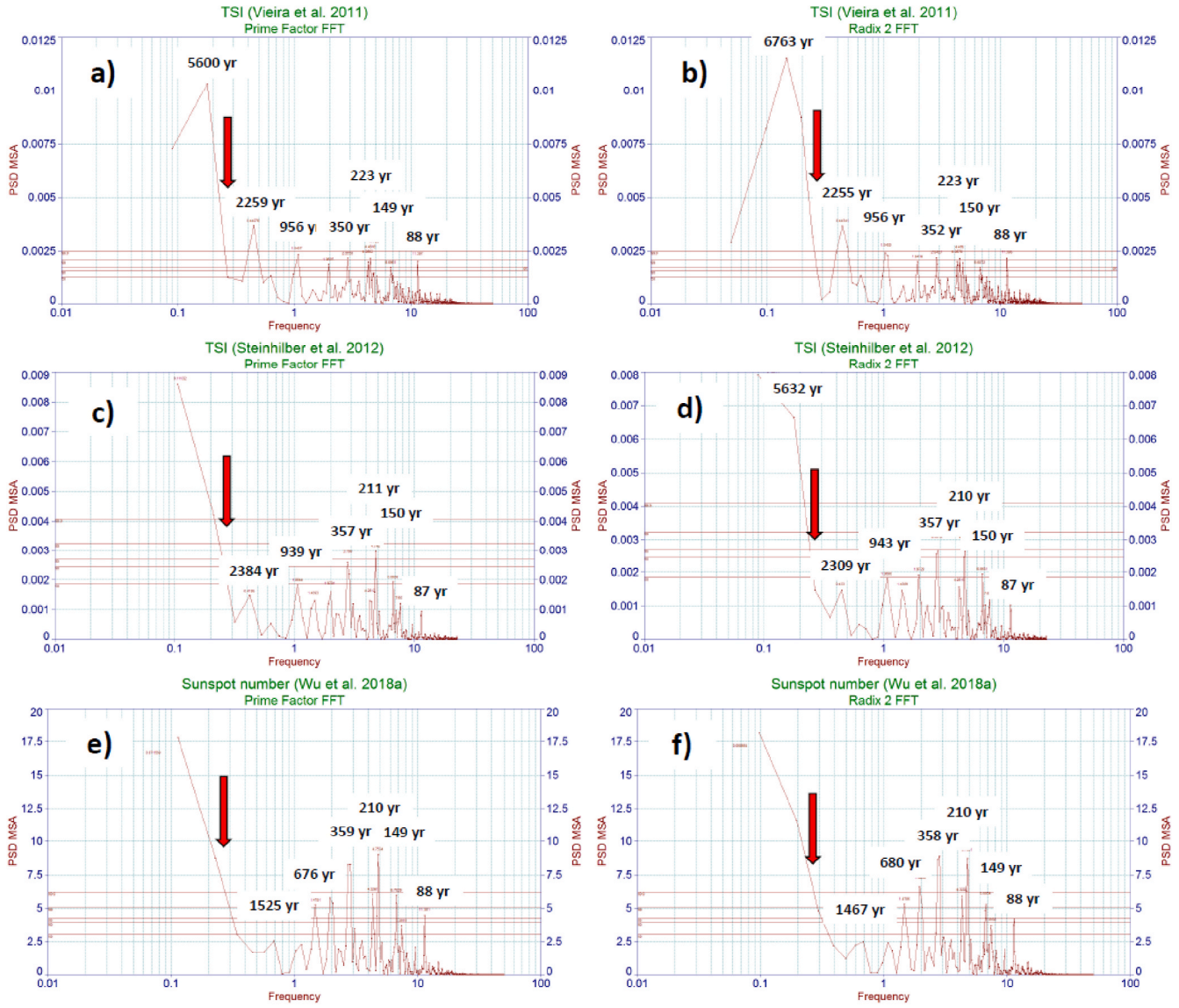

Fig. 4. Fourier frequency spectra with two different algorithms of selected detrended Holocene solar proxies: (**a-b**) TSI (Vieira et al., 2011); (**c-d**) TSI (Steinhilber et al., 2012); (**e-f**) sunspot number (Wu et al., 2018a). Prime factor FFT algorithm (left spectra), Radix 2 FFT algorithm (right spectra) (SeaSolve, 2003). The red arrows indicate the frequency region of the 3.4–3.6-kyr cycle.

system effects which influence the radionuclide signal (e.g. climate-induced transport and deposition changes, changes in the carbon cycle) (Mayewski et al., 1997; Solanki et al., 2004; Steinhilber et al., 2012; Charvátová and Hejda, 2014; Usoskin, 2017). Within the range of the sub-Milankovitch bands detected in the EPICA records (from 13 kyr to 2.5 kyr), and considering the temporal extension limit of the studied Holocene solar proxies (Vieira et al., 2011; Steinhilber et al., 2012; Wu et al., 2018a) in recording the ~9–10 kyr cycle, the FFS identifies a long-term cycle of 5.6–6.76 kyr (mean 6.2 kyr) from the TSI data of Vieira et al. (2011) (Fig. 4a and b), and of 5.6 kyr from TSI data of Steinhilber et al. (2012) (Fig. 4d). This cycle has also been recognized by Savitzky-Golay filtering, showing long-term TSI cycles in the range of 5.0–6.5 kyr, which is equivalent to a mean cycle of 5.6 kyr (Fig. 5). A stable TSI cycle of 2.3–2.4 kyr is recognizable by the frequency spectra, while the ~3.4–3.6 kyr cycle appears to be completely absent from the solar proxies (Fig. 4).

3.2.1. *EPICA 9.7-kyr cycle*

SA oscillations were analysed by Sánchez-Sesma (2015, 2016) and extrapolated based on reconstructed solar-related ^{14}C and ^{10}Be records. The author reported ~9.5-kyr solar patterns, and linked this SA cycle to a planetary gravitational forcing (PGF) affecting solar dynamo mechanisms originated by a 5:1 resonance (9.56 kyr) between the inner and outer planets secular frequencies and the solar periodicity detected. Sánchez-Sesma (2016) presented a qualitative verification of the TSI ~9.5-kyr recurrent patterns with an explosive demographic expansion of bivalve *Sinucongeria primiformis* in a Tortonian lacustrine system of Lake Pannon obtained from data by Harzhauser et al. (2013), showing the geological-scale persistence of the SA patterns, which can be explained by a PGF. Elrick and Hinnov (2007) investigated 17 different Paleozoic rhythmite successions from across North America. The rhythmic alternation between carbonate-rich and carbonate-poor layers is interpreted as millennial-scale paleoclimatic changes (~11–13; ~9.0; ~5–6; 3.0–3.8 and 2.1–2.3 kyr) of the Earth's ocean–atmosphere system, which points to an external driver such as solar forcing. Wu et al. (2012) reported 8.9–10.0 kyr cycles from South China Early Triassic rock magnetic cyclostratigraphy.

EPICA DCM component-7-8s all exhibit periodicities of 9.2 kyr, 9.8 kyr and 9.0 kyr, respectively. These oscillations are equivalent to an EPICA stack of 9.7 kyr, which is very close to the ~9.5-kyr SA oscillation

Table 3
Quantitative estimation of signal magnitude (percentage variance) and Fourier frequency results of the nine EPICA CH_4 components isolated by singular spectrum analysis. Interpretation of the suborbital forcings in the section "New Evidence of Solar Cycles from EPICA records". Unless otherwise indicated, the frequency peaks are the most significant peaks above a 99.9% critical limit. EPICA original data from Past interglacials working group of PAGES (2016).

CH_4 component rank	CH_4 component variance	Frequency (kyr^{-1})	TISA power (%)	Period (kyr)	Weighted mean period (kyr)	Forcing
1	44.7%	0.01037445	83.5	96		Short eccentricity (with obliquity modulation cycle)
		0.00607497	14.3	165		
		0.02080875	2.2	48	low significance	
2	27.5%	0.02462184	47.5	41		Obliquity with short eccentricity envelopes
		0.01042284	30.7	96		
		0.01339629	21.8	75		
3	9.3%	0.04517588	42.0	22		Precession and obliquity
		0.03424407	33.2	29		
		0.02464058	24.8	41		
4	5.2%	0.04532866	39.0	22	20	Precession
		0.05268014	24.6	19		
		0.05775437	36.4	17		
5–6	5.3%	0.07126878	19.4	14.0	13	Half-precession
		0.07579715	50.8	13.2		
		0.08269068	29.8	12.1		
7–8	2.6%	0.10377296	61.0	9.6	9.0	Sun
		0.11101707	17.1	9.0		
		0.13985521	21.9	7.2		
9–15	3.8%	0.15918553	29.5	6.3	5.4	Sun
		0.17518809	36.6	5.7		
		0.22862689	33.9	4.4		
16–23	1.0%	0.25310536	37.4	4.0	3.6	Unclear
		0.29041320	25.9	3.4		
		0.29438171	36.7	3.4		
24–26	0.2%	0.39871067	26.1	2.5	2.5	Sun
		0.40341315	29.0	2.5		
		0.40681530	44.9	2.5		
>26	0.4%					Noise

found by Sánchez-Sesma (2016), and to the 8.9–9.2-kyr solar-related cycle of Elrick and Hinnov (2007). However, some studies report a 9.0–9.5-kyr quasi-period, which is interpreted as nonlinear harmonics or combination tones of primary Milankovitch cycles (Pestiaux et al., 1988; Franco and Hinnov 2012; Franco et al., 2012), showing an apparent 'multi-forcing' beat (Table 4).

3.2.2. *EPICA 6.0-kyr cycle*

Mayewski et al. (1997) provide indications of a 6.1-kyr cycle from the Greenland Ice Sheet Project 2 (GISP2) glaciochemical series of the last 110,000 years, and found a very strong association with the timing of Heinrich events (H). These last glacial H0–H6 events are North Atlantic marine layers rich in carbonate ice-rafted debris (IRD), which result from massive iceberg discharge and the attendant cooling of surface waters with a quasi-periodic return interval of ~6 kyr (Heinrich, 1988; Andrews et al., 1995; Alley, 1998; Bond et al., 2001; Hodell et al., 2008; Channell et al., 2012). Channell et al. (2012) extend a North Atlantic Heinrich-like detrital-layer stratigraphy at the Integrated Ocean Drilling Program (IODP) Sites U1302–U1303 (SE flank of Orphan Knoll, Labrador Sea) up to the last 750 kyr within a robust chronological framework, representing a history of iceberg discharges from the Laurentide Ice Sheet. Mayewski et al. (1997) interpret the 6.1-kyr cooling cycle as not being related solely to ice sheet dynamics, but also linked to other mechanisms that allow suborbital-scale changes in insolation, perhaps of solar origin, to be translated through the ocean-atmosphere-cryosphere system into climate changes. Xapsos and Burke (2009) analysed the reconstructed sunspot numbers reported by Solanki et al. (2004) based on ^{14}C in tree rings and ^{10}Be in ice cores. Their spectral result was a prominent peak of SA, equivalent to a period of 5.68 kyr not previously reported. Xapsos and Burke (2009) introduced the possibility that evidence of such a ~6.0-kyr solar cycle has been recorded in proxy data, such as the glaciochemical series reported by Mayewski et al. (1997) with indications of a 6.1-kyr cycle. Olsen and Hammer (2005) showed that between 45 and 11-kyr BP, semi-cycles of glacial fluctuations comparable to the Bond cycle bundles of Dansgaard-Oeschger cycles (DO) are recorded from both marine and terrestrial data obtained from Norway, and follow a cyclical pattern of ~6.0 kyr. The authors conclude that the causal mechanisms for the observed periodicity are not likely to be limited only to the internal processes in the Earth's climatic system, but that external forcing, such as periodic changes in the magnetic field, may be the primary cause. Bond et al. (1997, 2001) propose that changes in the flux of solar energy on a ~1.5-kyr scale may be correlated to the DO cycles, and in turn to the Heinrich events. The authors propose that Earth's climate system is highly sensitive to extremely weak perturbations in the Sun's energy output, and that the observed large effects require at least large positive feedback processes acting within the Earth's system. Wu et al. (2012) investigate rock magnetic cyclostratigraphy from the Early Triassic Lower Daye Formation (South China), and find a 4.7–5.6-kyr cycle interpreted as millennial-scale fluctuations in the solar output. Creer and Tucholka (1983) and Hagee and Olson (1989) have found geomagnetic secular variations of 5.0–5.8 kyr worldwide from Late Pleistocene-Holocene lacustrine sediments. Again, some studies report ~5.5–7.0-kyr oscillations interpreted as nonlinear harmonics or combination tones of primary Milankovitch cycles (Pestiaux et al., 1988; Da Silva et al., 2018), or as 4–5-kyr sun-planetary mass centre eccentricity beat (Scafetta et al., 2016), suggesting an apparent 'multi-forcing' nature of this cycle.

Antarctic DCM component-9-15s show periodicities of 5.7 kyr, 5.9 kyr and 5.4 kyr, matching an EPICA stack of 6.0 kyr. This is very close to the ~5.7-kyr SA cycle reported by Xapsos and Burke (2009), and to the ~5.8-kyr TSI mean cycle found in this study based on data reported by Vieira et al. (2011) and Steinhilber et al. (2012) (Figs. 4 and 5). It is also similar to ~5.0–6.0-kyr solar-related cycles found in literature (Mayewski et al., 1997; Bond et al. 1997, 2001, 2001; Olsen and Hammer, 2005; Elrick and Hinnov 2007; Wu et al., 2012).

3.2.3. *EPICA 3.7-kyr cycle*

Based on the recent literature on millennial-scale solar cycle proxies (Xapsos and Burke, 2009; Vieira et al., 2011; Steinhilber et al., 2012;

Table 4
Comparison of sub-Milankovitch cycles (in kyr) identified in the EPICA records by SSA (present work) with other signals and their interpretation (forcing) from literature. Despite large differences in signal type, sample resolution, age models and spectral methods, of note is the coupling of suborbital cycles with similar quasi-periods across solar proxies (sun electromagnetic activity), geomagnetic secular variations, paleoclimate oscillations, nonlinear harmonics or combination tones of primary Milankovitch cycles, and resonant planetary beats.

Signal	Age	sub-Milankovitch cycle				
EPICA stack [m]	Middle Pleistocene-Holocene	13	9.7	6.0	3.7	2.5
EPICA δD [m]	Middle Pleistocene-Holocene	13	9.2	5.7	3.4	2.4
EPICA CO_2 [m]	Middle Pleistocene-Holocene	13	9.8	5.9	3.6	2.5
EPICA CH_4 [m]	Middle Pleistocene-Holocene	13	9.0	5.4	3.6	2.5
LR04 $\delta^{18}O$	Pliocene-Pleistocene	13 [d]	–	–	–	–
ODP Site 846 SST	Pliocene-Pleistocene	12 [d]	–	–	–	–
Lithological rhythm	Lower Kimmeridgian	13–14 [e]	–	–	–	–
GISP2 glaciochemical series [i]	Late Pleistocene-Holocene	11.1	–	6.1	3.2	2.3
Dates distribution of ice-free intervals [j]	Late Pleistocene	–	–	6.0	–	–
Solar proxies (^{14}C; ^{10}Be)	Middle Pleistocene-Holocene	–	9.5 [a]	5.0–6.7 [b]	–	2.2–2.7 [b,q]
Solar background magnetic field [o]	Late Pleistocene-Holocene	–	–	–	–	2.0–2.1
Indian Ocean $\delta^{18}O$ [f]	Late Pleistocene	12.8–13	9.1–9.3	5.6–5.9	2.7–3.7	2.5
Rhythmites cyclostratigraphy [k]	Paleozoic	11.0–12.7	8.9–9.2	4.7–6.0	3.0–3.8	2.1–2.3
Rhythmites (coupled thickness and magnetostratigraphy) [l]	Late Carboniferous-Early Permian	11.1–13.6	8.8–10	5.1–6.2	3.4–3.6	2.4–2.7
Rock magnetic cyclostratigraphy [g]	Early Triassic	12.3–12.6	8.9–10.0	4.7–5.6	3.8	–
Geomagnetic secular variations [c]	Late Pleistocene-Holocene	13.5	–	5.0–5.8	3.0–3.8	2.1–2.6
Titanium cyclostratigraphy [h]	Early Devonian	10–12	–	6–7	–	2.5
Orbit of the planetary mass center relative to the Sun [n]	Late Pleistocene-Holocene	–	–	4–5	–	2.3
Forcing	**Age**	**sub-Milankovitch cycles**				
Solar activity	–	11–13 [k]	~9.0 [k]	5–6 [b,g,i,j,k]	3.0–3.8 [k]	2.2–2.7 [b,h,i,k,l,m,q]
Planetary beat on Sun	–	–	9.6 [a]	4–5 [n]	–	2.1–2.4 [n,o,p,q]
Nonlinear Milankovitch oscillator [f]	–	12.4–13	9.0–9.5	5.5–5.8	2.9–3.1	2.3–2.7
Combination tones of Milankovitch cycles	–	10–12 [h]	9.2 [l]	6–7 [h]	–	–
AM of Milankovitch cycles	–	13.9 [e]	–	–	–	–
Intertropical half-precession	–	11–13 [d,g,l]	–	–	–	–

[a] Sánchez-Sesma (2015, 2016).
[b] Dergachev (2004); Xapsos and Burke (2009); present study from data of Vieira et al. (2011) and Steinhilber et al. (2012); Usoskin et al. (2016); Usoskin (2017).
[c] Creer and Tucholka (1983); Hagee and Olson (1989); Gogorza et al. (2000).
[d] Viaggi (2018).
[e] Rodrìguez-Tovar and Pardo-Igùzquiza (2003).
[f] Pestiaux et al. (1988).
[g] Wu et al. (2012).
[h] Da Silva et al. (2018).
[i] Mayewski et al. (1997).
[j] Olsen and Hammer (2005).
[k] Elrick and Hinnov (2007).
[l] Franco and Hinnov (2012); Franco et al. (2012).
[m] This work.
[n] Scafetta et al. (2016).
[o] Zharkova et al. (2019).
[p] Charvátová (2000).
[q] McCracken et al. (2014).

Sánchez-Sesma, 2016; Usoskin et al., 2016; Wu et al., 2018a), of note is the absence of the periodicity at ~3.6 kyr (Table 4). The FFS analysis performed in the present study on some Holocene solar proxies (Fig. 4) shows that the frequency region between 0.28 and 0.30 cycles per kyr has no peaks, thus confirming the possible absence of the ~3.6-kyr cycle in solar proxies. Instead, a trace of this oscillation is reported in the glaciochemical GISP2 polar atmospheric circulation index at 3.2–3.6 kyr as a >99% significant level cycle (Fig. 3 in Mayewski et al., 1997). A strong period of ~3.6 kyr in ^{10}Be deposition rates from Vostok ice-core raw data was detected by Omerbashich (2006), and was interpreted as an extrasolar galactic-burst signature. It is interesting to note that Gogorza et al. (2000) found secular variations of 3.4 kyr in the declination and inclination of the geomagnetic field from four lake sediment records in south-western Argentina. The oscillations are characterized by alternating clockwise and counter-clockwise looping of the geomagnetic vectors during the last 6700 years. Other authors have found similar geomagnetic secular variations of 3.0–3.8 kyr worldwide (Creer and Tucholka, 1983; Hagee and Olson, 1989). The North America Paleozoic 3.0–3.8-kyr rhythmic alternation between carbonate-rich and carbonate-poor layers, is interpreted as solar-related paleoclimatic changes of the Earth's ocean–atmosphere system (Elrick and Hinnov 2007). Pestiaux et al. (1988) demonstrate that a 2.9–3.1-kyr periodicity may be the result of a nonlinear oscillator of primary Milankovitch frequencies.

In summary, EPICA DCM component-16-23s exhibit a 3.4-kyr atmospheric temperature and 3.6-kyr GHG oscillation, matching an EPICA stack of 3.7 kyr, apparently absent from solar proxies, and close to a geomagnetic secular variation of 3.0–3.8 kyr (Creer and Tucholka, 1983; Hagee and Olson, 1989; Gogorza et al., 2000; Wu et al., 2012), as well as close to 2.9–3.1-kyr beat of nonlinear Milankovitch oscillator (Pestiaux et al., 1988). Therefore, this cycle does not seem to be of solar origin, although a gravitational forcing cannot be ruled out.

3.2.4. EPICA 2.5-kyr cycle

SA at 2.31 ± 0.30 kyr is known in literature as the Hallstatt cycle (Dergachev, 2004; Xapsos and Burke, 2009; Steinhilber et al., 2012; Sánchez-Sesma, 2016; Usoskin et al., 2016; Usoskin, 2017). The wavelet spectrum of TSI shows that the de Vries cycle (210 yr) amplitude has varied with a period of about 2.2 kyr, and is called the Hallstatt cycle (Steinhilber et al., 2012). A stable TSI cycle of 2.3–2.4 kyr is also recognizable by the FFS employed in the present study (Fig. 4). Despite some initial interpretative uncertainties, the Hallstatt cycle is currently considered to be of solar origin, and is manifested through clustered occurrence of grand minima and grand maxima around its minima and

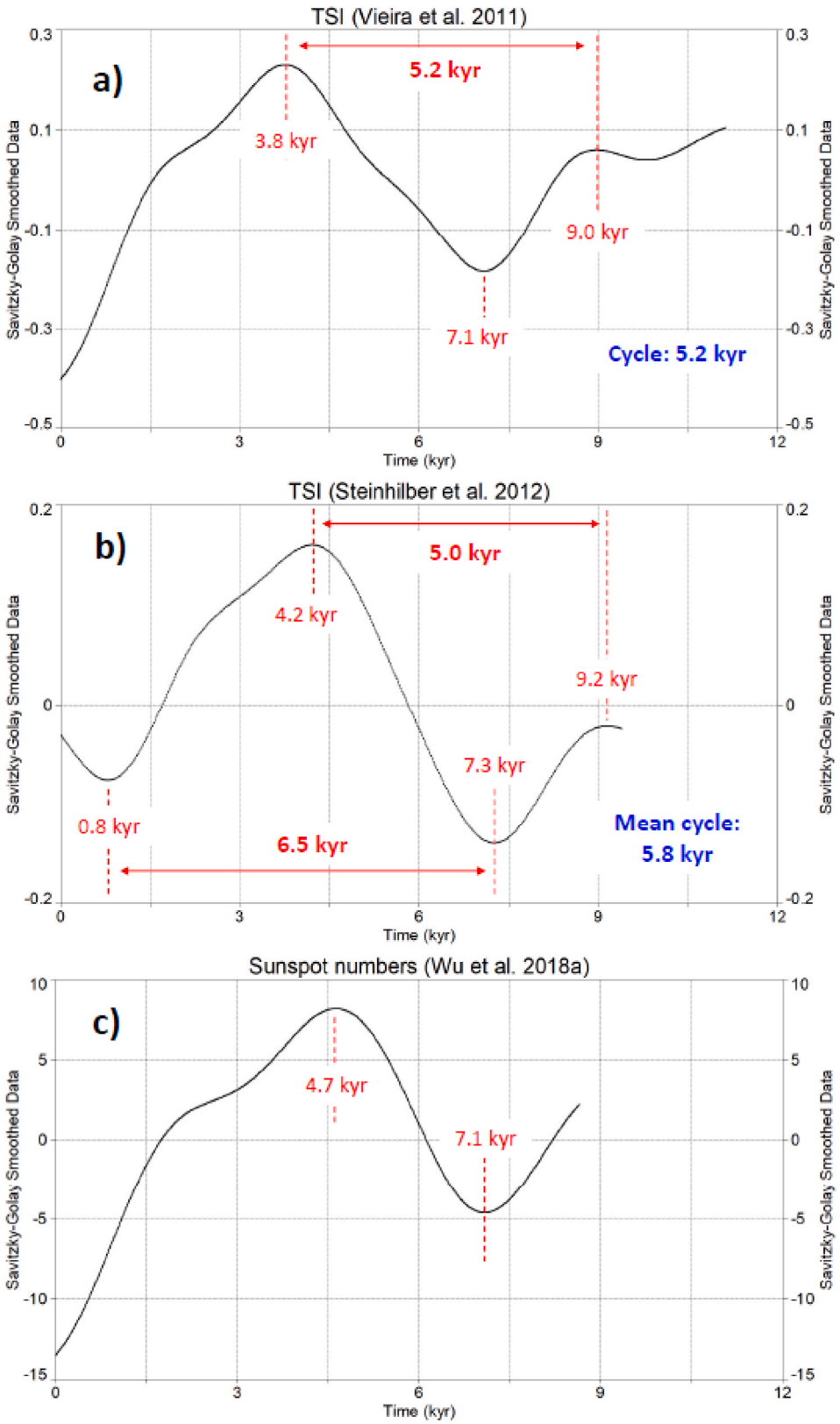

Fig. 5. Long-term smoothing by Savitzky-Golay filter of selected detrended Holocene solar proxies: (**a**) TSI (Vieira et al., 2011); (**b**) TSI (Steinhilber et al., 2012); (**c**) sunspot number (Wu et al., 2018a). Notably, the long-term Sun-related cycles are in the range 5.0–6.5 kyr, which is equivalent to a mean cycle of 5.6 kyr, close to the EPICA stack ~6.0-kyr cycle. The possible Sun-related cycles are discussed according to descending period in the following sections.

maxima, respectively, indicating that the Hallstatt cycle is a long-term feature of SA that needs to be considered in solar dynamo models (Steinhilber et al., 2012; Usoskin et al., 2016; Usoskin, 2017). Interestingly, McCracken et al. (2014) and Scafetta et al. (2016) show that this oscillation is coherent to a repeating pattern in the periodic revolution of the four Jovian planets (Jupiter, Saturn, Uranus, and Neptune) around the Sun, which has a stable resonance period of ~2.3 kyr, supporting PBH. Even Zharkova et al. (2019) found oscillations of ~2.1 kyr of the baseline of a solar magnetic field close to the Hallstatt cycle, and this is likely to be caused by the SIM about the barycentre of the solar system caused by large planets, and affecting the TSI. Pestiaux et al. (1988) show a 2.5-kyr cycle from Indian Ocean $\delta^{18}O$ interpreted as the 2.3–2.7-kyr nonlinear response of a Milankovitch oscillator. The Hallstatt cycle is found in a number of sedimentary signals through the geological record: from North America Paleozoic rhythmite successions (2.1–2.3 kyr) (Elrick and Hinnov 2007); from glaciogenic rhythmites (coupled thickness and magnetostratigraphy) from the Brazil Late Paleozoic Itararé Group (2.4–2.7 kyr) (Franco and Hinnov 2012; Franco et al., 2012); from Early Devonian Titanium cyclostratigraphy (2.5 kyr) (Da Silva et al., 2018) and from Greenland Late Pleistocene-Holocene GISP2 glaciochemical series (2.3 kyr) (Mayewski et al., 1997). It should be noted that Hallstatt-like cyclicity of 2.1–2.6 kyr has been observed worldwide from Late Pleistocene-Holocene geomagnetic secular variations (Creer and Tucholka, 1983; Hagee and Olson, 1989; Gogorza et al., 2000). Antarctic DCM component-24-26s exhibit oscillations at 2.4 kyr, 2.5 kyr and 2.5 kyr, which are equivalent to an EPICA stack of ~2.5 kyr, close to the 2.31 ± 0.30-kyr period known in literature as the Hallstatt cycle. Finally, the phase relationships determined by cross-spectral analysis (details in Additional file 1, section 4) indicate an excellent coherence (0.93) between the EPICA stack 2.5-kyr cycle and the Hallstatt TSI wavelet filtered signal from data of Steinhilber et al. (2012) in the common band at ~2.3-kyr, with a phase lags of EPICA response of about 130 yr. These results confirm that the EPICA stack 2.5-kyr is a good quality signal with a solar origin linked to the Hallstatt cycle.

3.3. 'Multi-forcing' beat of the suborbital cycles: the Hallstatt cycle case

As previously discussed with the support of Table 4, despite the large differences in signal type, sample resolution, age models and spectral methods, it is interesting to note an apparent coupling of suborbital cycles with similar quasi-periods across solar proxies (sun electromagnetic activity), geomagnetic secular variations, paleoclimatic oscillations, nonlinear harmonics or combination tones of primary Milankovitch cycles, and resonant planetary beats. This suggests an intriguing hypothesis of a multifaceted effect of the planetary gravitational forcing. For discussion purposes, we focus on the well-known ~2.3-kyr Hallstatt cycle, which is currently interpreted to be a property of the millennial-scale SA. As such, it is logical to expect its occurrence even in paleoclimatic-related sedimentary signals, as attested by literature (Mayewski et al., 1997; Elrick and Hinnov 2007; Da Silva et al., 2018) and documented in the present work by Antarctic records. However, Hallstatt-like cyclicity has also been recognized as a Jovian planets beat resonance (McCracken et al., 2014; Scafetta et al., 2016; Zharkova et al., 2019) and as a nonlinear response of the Milankovitch oscillator (Pestiaux et al., 1988), which pose striking interpretative questions. In addition, it is unclear how it explains Hallstatt-like cycles even in worldwide geomagnetic secular variations (Creer and Tucholka, 1983; Hagee and Olson, 1989; Gogorza et al., 2000). Higher-frequency geomagnetic variations are generally considered to be external in origin (e.g. daily variations due to the Earth's rotation, variations due to changes in SA and interactions between the solar wind and the magnetic field), whereas the long-period geomagnetic field variability could originate in the geodynamo (e.g. sudden acceleration of the metallic fluid flow at the boundary of the Earth's outer core; torsional oscillations in the Earth's core) and is known as the geomagnetic secular variation (De Michelis et al., 2005; Roberts and Turner, 2013). However, the cut-off between these two domains may not be as distinct as is sometimes argued (De Michelis et al., 2005). The Earth can be considered a probe reacting to interplanetary disturbances, which are manifestations of the solar magnetic fields, and thus records of the geomagnetic activity may be used as diagnostic tools for reconstructing the evolution of previous solar magnetic fields (Georgieva et al., 2013). The authors find the correlations between the geomagnetic activity and the 11-yr sunspot magnetic cycle, and estimate the variations in the sunspot magnetic field from geomagnetic data. Can the solar activity of the Hallstatt cycle affect the geomagnetic field by modulating Hallstatt-like geomagnetic secular variation ? The study of secular variations in the geomagnetic field helps to determine both physical and chemical properties of the Earth's interior and the fluid flow of the outer-core (Liu et al., 1999; De Michelis et al., 2005). Geomagnetic secular variations have been found to undergo rapid accelerations (geomagnetic Jerk), which can provide constraints on the deep mantle conductivity. The variation in the fluid flow in the outer-core caused by the core-mantle coupling is a plausible explanation of the changes in geomagnetic Jerk (Liu et al., 1999). The Jerk is related to the core-mantle electromagnetic coupling, and may be caused by the Earth's angular momentum (Liu et al., 1999). One could therefore speculate that the ~2.3 kyr gravitational stress of the planetary system (McCracken et al., 2014; Scafetta et al., 2016; Zharkova et al., 2019) affect the geodynamo through the Earth's angular momentum (Mörner, 2013). PBH is a fascinating hypothesis that has the potential to unify the apparent contradictions of 'multi-forcing' suborbital cycles. However, there is the need for in-depth studies related to the understanding of the physical processes that would regulate the electromagnetic activity of the Sun (McCracken et al., 2014; Scafetta 2012, 2014b; Zharkova et al., 2019) and the possible direct and indirect effects on the Earth, especially considering the very low magnitude of the planetary gravitational beat.

3.4. Recurrence analysis of Heinrich events vs. sun-related cycles

A variety of mechanisms have been proposed to explain Heinrich events generally in terms of internal variability of ice sheets. One of these mechanisms is the "binge-purge" model stating that as an ice sheet thickens, it acts as an insulator trapping geothermal and frictional heat at its base (MacAyeal, 1993). Once the pressure melting point is reached, the melted unconsolidated base acts as a slip plane resulting in surging. Channell et al. (2012) note that the detrital layers at the Sites U1302–U1303 are distributed in both glacial and most interglacial stages, although interglacial detrital layers are not always associated with IRD and may include a component deposited from suspension derived from Northwest Atlantic Mid-Ocean Channel-related turbidity currents and flood events. Heinrich-like detrital layers in peak glacial stages are bunched into groups with a persistent ~6–10 kyr recurrence time, possibly related to cyclic changes in basal temperature of the Laurentide Ice Sheet (Channell et al., 2012). Fig. 6 exhibits a new recurrence analysis of Heinrich and Heinrich-like events obtained from age data published by Channell et al. (2012) on Sites U1302/03 within a robust chronological framework (Table 5). The mean age is reported when multiple dating is available from different sites. The Sites U1302/03 age model is built by tandem matching of relative geomagnetic paleointensity and $\delta^{18}O$ data from *Neogloboquadrina pachyderma* (sin.) to reference records to improve the resolution of stratigraphic correlation, the reference curves being the relative geomagnetic paleointensity stack (Channell et al., 2009) and the LR04 benthic $\delta^{18}O$ stack (Lisiecki and Raymo, 2005). The age model enables correlation of Sites U1302/03 to IODP Site U1308 in the heart of the central Atlantic IRD belt. Ages of Heinrich layers H1, H2, H4, H5 and H6 are within ~2 kyr at the two sites (H0, H3 and H5a are not observed at Site U1308), and agree with previous work at Orphan Knoll within ~3 kyr (Channell et al., 2012). Twenty Heinrich and Heinrich-like events (10 consecutive pairs of min or max) of the Sites U1302/03 have an average recurrence time of

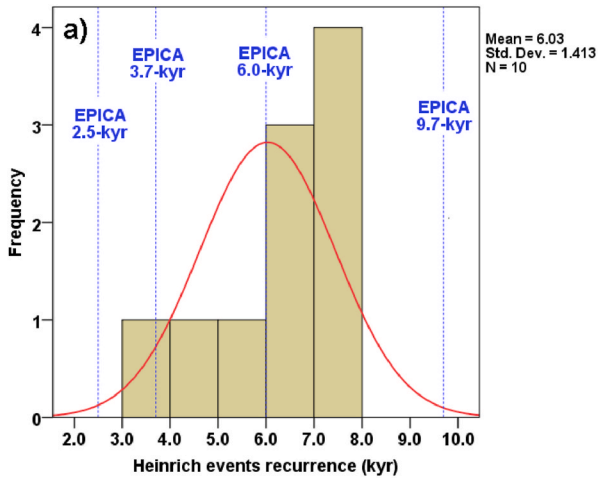

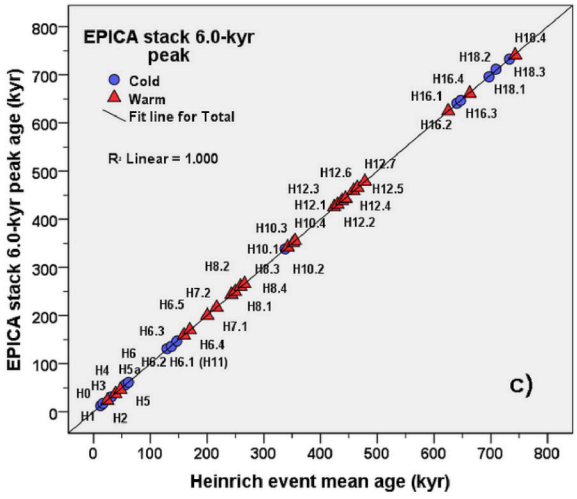

b)

Heinrich events recurrence
One-Sample Test

Test Value = EPICA 9.7 kyr cycle					
				95% Confidence Interval of the Difference	
t	df	Sig. (2-tailed)	Mean Difference	Lower	Upper
-8.2	9	.000	-3.6700	-4.681	-2.659

One-Sample Test

Test Value = EPICA 6.0 kyr cycle					
				95% Confidence Interval of the Difference	
t	df	Sig. (2-tailed)	Mean Difference	Lower	Upper
.067	9	.948	.0300	-.981	1.041

One-Sample Test

Test Value = EPICA 3.7 kyr cycle					
				95% Confidence Interval of the Difference	
t	df	Sig. (2-tailed)	Mean Difference	Lower	Upper
5.21	9	.0006	2.3300	1.319	3.341

One-Sample Test

Test Value = EPICA 2.5 kyr cycle					
				95% Confidence Interval of the Difference	
t	df	Sig. (2-tailed)	Mean Difference	Lower	Upper
7.897	9	.000	3.5300	2.519	4.541

Fig. 6. Recurrence analysis of Heinrich and Heinrich-like events from age data of Channell et al. (2012); (**a**) Histogram and descriptive statistics of the recurrence time of 10 consecutive pairs of min or max compared to the suborbital cycles of EPICA stack signals (2.5-, 3.7-, 6.0- and 9.7-kyr); (**b**) One-sample *t*-test of Heinrich events 6.03 kyr mean recurrence time, showing its statistical proximity to the ~6.0-kyr cycle of EPICA with respect to the 9.7-kyr, 3.7-kyr and 2.5-kyr cycles, which significantly differ from the recurrence time of Heinrich events; (**c**) Age crossplot between the Heinrich events and the nearest 6.0-kyr peaks of EPICA stack signal and their polarity (Table 5). EPICA original data from Past interglacials working group of PAGES (2016).

6.03 ± 1.4 kyr, which is close to the ~6.0-kyr Sun-related cycle of the EPICA stack signal (Fig. 6a), as supported by statistical tests (Fig. 6b). In fact, the one-sample *t*-test shows the Heinrich events recurrence time of 6.03 kyr to be statistically close to the ~6.0-kyr cycle of EPICA with respect to the other 9.7-kyr, 3.7-kyr and 2.5-kyr EPICA cycles, which significantly differ from the recurrence time of Heinrich events. These results are consistent with those known in literature, which indicate a quasi-periodic return interval of ~6 kyr (Heinrich, 1988; Andrews et al., 1995; Mayewski et al., 1997; Alley, 1998; Bond et al., 2001; Hodell et al., 2008; Channell et al., 2012). Fig. 6c shows the age crossplot between the Heinrich events and the nearest 6.0-kyr peak of the EPICA stack signal (Table 5).

The proposed correlation pattern of the Heinrich and Heinrich-like events with EPICA stack ~6.0-kyr cycle shown in Fig. 7, as well as in Fig. 8 for the last 60,000 years, is basically in agreement with that of Channell et al. (2012) which recognise Heinrich-like events even in an interglacial context, along with the common notion that Heinrich events occur toward the end of glacial cycles as cold-related events. Despite the inevitable inaccuracies due to age model differences, the nearest-6.0 peak correlation criterion should produce non-systematic errors in the definition of the polarity of the cycle. Although the alleged polarity of some correlated Heinrich events may therefore not be correct, the fact that a large number of events (~63%), and especially those of Heinrich-like events, can be traced back to the heating phases of the Sun-related ~6.0-kyr cycle, could suggest destabilization of the ice-sheet for surface heating and meltwater runoff/ice front disruption ('warm-related' Heinrich event). These processes may have favoured meltwater streams and the deposition of mud suspensions associated to turbiditic currents and flood events as observed by Channell et al. (2012) in the North Atlantic region. This interpretation is in agreement with that of Turney et al. (2004), which correlate three periods of increasing 'warm' El Nino/Southern Oscillation (ENSO) activity identified from Lynch's crater record (northern Queensland, Australia) with H1, H2 and H4 events in the GISP2 $\delta^{18}O$, although H1 does not match the same polarity proposed in EPICA. One explanation for the relationship between ENSO states and Heinrich events is that during an El Nino phase, there is warming on a northwest–southeast transect across North America, causing the potential melting of an ice front (Turney et al., 2004). On the other hand, as proposed by Hodell et al. (2008), the 'cold-related' Heinrich events may result from instability associated with excess ice and frictional heat at its base leading to increase of ice calving process and IRD-layers.

According to Channell et al. (2012), the prominent detrital layers at Sites U1302/03 and U1308 may be correlated to millennial-scale features in the Chinese speleothem record over the last 400 kyr, implying a link between monsoon precipitation and Laurentide Ice Sheet instability. Fig. 8 also exhibits the approximate correlation of EPICA Sun-related (~9.7-kyr; ~6.0-kyr; ~2.5-kyr) and ~3.7-kyr signals with

Table 5
Dating of Heinrich events (H0–H6) and Heinrich-like events of the Sites U1302/03 (data from Table 1 of Channell et al., 2012) and comparison with the ages of plausibly correlative features of EPICA stack nearest-6.0 kyr cycle and their climate polarity. The age is reported as the mean age (with standard deviation) when multiple dating are available from different sites (Core HU91-045-94P, Orphan Knoll; Core MD95-2024, Orphan Knoll; Site U1308; Chinese speleothem record).

Heinrich event	Heinrich age (kyr)	Std. Dev. (kyr)	EPICA near-6.0 peak age (kyr)	EPICA Cold/Warm peak
H0	12.3	0.4	12.5	C
H1	16.5	0.8	17.5	C
H2	24.4	1.2	23.5	W
H3	30.8	1.8	30.5	C
H4	38.7	1.8	37.5	W
H5	47.3	1.4	46.0	W
H5a	55.7	2.7	56.0	C
H6	61.6	1.9	61.5	C
H6.1 (H11)	129.6	1.6	131.0	C
H6.2	137.1	2.2	136.0	C
H6.3	146.9	3.7	147.0	C
H6.4	159.4	3.4	159.5	W
H6.5	169.6	0.9	170.0	W
H7.1	200.5	1.1	200.0	W
H7.2	216.9	1.0	217.0	W
H8.1	243.0	0.8	243.5	W
H8.2	249.6	0.3	249.5	W
H8.3	259.0	–	260.5	W
H8.4	266.0	–	266.0	W
H10.1	337.7	1.2	338.5	C
H10.2	342.0	–	342.0	W
H10.3	352.0	–	351.0	W
H10.4	355.0	–	355.5	W
H12.1	424.0	–	425.5	W
H12.2	430.0	–	430.5	W
H12.3	438.0	–	438.5	W
H12.4	444.0	–	443.0	W
H12.5	458.0	–	459.5	W
H12.6	465.0	–	465.5	W
H12.7	478.0	–	478.5	W
H16.1	625.0	–	624.5	W
H16.2	640.0	–	641.0	C
H16.3	647.0	–	646.5	C
H16.4	663.0	–	661.0	W
H18.1	697.0	–	696.0	C
H18.2	709.0	–	711.5	C
H18.3	733.0	–	732.5	C
H18.4	743.0	–	741.0	W

NGRIP $\delta^{18}O$ (NGRIP Community Members, 2007) and North Atlantic glaciological events: Greenland Stadials (GS) from Rasmussen et al. (2014) and Dansgaard-Oeschger cycles from EPICA Community Members (2006). As discussed in the previous section, the occurrence in solar proxies of a ~5.7-kyr SA cycle from reconstructed sunspot numbers reported by Xapsos and Burke (2009), as well as a ~5.8 kyr TSI mean cycle found in this study from data presented by Vieira et al. (2011) and Steinhilber et al. (2012) (Figs. 4 and 5), support a Sun-related origin of the EPICA ~6.0-kyr cycle. According to the recurrence analysis of Heinrich events and their correlation with EPICA ~6.0-kyr oscillation, it is proposed to name this plausible band of SA as the 'Heinrich-Bond cycle' because Heinrich (1988) and Bond et al. (1993) first noted the occurrence of IRD layers linked to SST from North Atlantic sediments. On the basis of the correlations made in this study and the results of Channell et al. (2012), it is deemed that the 'Heinrich-Bond' solar cycle may act on the ice-sheet as an external instability factor both related to excess ice and basal frictional heat which increase the ice-calving process ('cold-related' Heinrich events), and surface heating with meltwater streams ('warm-related' Heinrich events). This interpretation does not disagree with the "binge-purge" model because it introduces a possible external control to variations in the thickness of the ice-sheet and its instability in both cold and warm phases of the 'Heinrich-Bond' ~6.0-kyr Sun-related cycle.

3.5. Quantitative impact of EPICA components by forcing

The quantitative ranking of the Pleistocene climate responses by forcing is summarized in this section. Table 6 shows the quantitative impact of the EPICA reconstructed responses by forcing for the last 800,000 years. Figs. 9 and 10 show the time-series panel of δD, CO_2, CH_4 and stack signals by forcing with their magnitude as % variance. It is important to highlight that the signal strength obtained by variance is a relative concept, and is inversely proportional to the total variance of the time series which was investigated, and thus to its temporal extension. Therefore, for a short time series, the same signal exhibits a strength that appears to be more relevant compared to a long record because of the former 'defect' in total variance due to the lack of high-order cycles or long-term trend. For this reason, the variance strength of the 800,000-yr-long EPICA records is apparently higher than that shown by Viaggi (2018) in the Pliocene-Pleistocene global $\delta^{18}O$ and equatorial SST signals, and this is because of the absence of long-term trend components in current EPICA records. Each component is discussed by forcing in the following lines.

Mid-term oscillation - All of the studied EPICA signals exhibit a mid-term oscillation showing a mild warming phase centred at ~400 kyr, which correlates to the wide swing of LR04 $\delta^{18}O$ long-term component depletion at ~400-300 kyr, referred to as MBO (Viaggi, 2018). This mid-term oscillation is not related to the long eccentricity 400-kyr cycle (Laskar et al., 2011). The δD and CH_4 variance fractions driven by this mid-term component are 2.0% and 3.5%, respectively, and reach the CO_2 maximum value of 7.7%. The mean variance for the stack signal is 4.4%. This Antarctic mid-term component is here considered as a trace of the final stage of the Plio-Pleistocene long-term trend component (Viaggi, 2018), which cannot be registered in the current EPICA record. Viaggi (2018) observes the Late Pleistocene was a period of quiescence of the circum-Pacific explosive activity (Jicha et al., 2009) a possible cause of the MBO. In fact, the feedback mechanism related to the reduced supply of ash that fertilized the Pacific Ocean waters might have mitigated algal growth and CO_2 uptake (Jicha et al., 2009; Viaggi, 2018). The MBO peak supports the hypothesis that MIS-11, which is not proportional to eccentricity (Imbrie et al., 1993) or cool insolation-induced interglacials (Luthi et al., 2008; Berger and Yin, 2012; Berger et al., 2012; Past interglacials working group of PAGES, 2016), may be an astronomical event boosted by this GHG mid-term recovery (Viaggi, 2018). The main difference in this interpretation compared to the literature lies in attributing the amplitude 'boosting' at least in part to a specific long-term component of the climate system, whose most recent expression is the MBO.

Obliquity amplitude modulation cycles – The DCM signals all exhibit a ~160-240-kyr periodicities superposed to the mid-term components, for which a 2.5–5.8% variance may be estimated. The mean variance on the stack signal is 4.0%. These oscillations may be linked to the obliquity amplitude modulation cycles (~160–200 kyr) (Boulila et al., 2011) recognized by Viaggi (2018) also in the Pliocene-Pleistocene global $\delta^{18}O$ and equatorial ODP Site 846 SST records.

Short eccentricity – As expected in a post-MPT record, the short eccentricity is primarily responsible for the variance of the EPICA components being estimated as 50.5% (δD), 58.9% (CO_2) and 45.5% (CH_4), and is equivalent to a stack mean variance of 51.6%.

Obliquity – this band of orbital frequencies accounts for a variance of 23.4% (δD), 11.9% (CO_2) and 21.7% (CH_4). The mean variance on the stack signal is 19.0%.

Precession - The variance driven by precession may be estimated to be within the range 5.9–9.9%, which is equivalent to a stack mean variance of 8.4%.

Half-precession - A 2.5–5.3% range in variance is paced by the ~13-kyr cycle related to the half-precession band of equatorial origin. Other studies demonstrated that the effect of the half-precession cycle could be transferred from lower latitudes to higher latitudes via seawater surface and atmospheric heat advection (Hagelberg et al., 1994; Turney et al.,

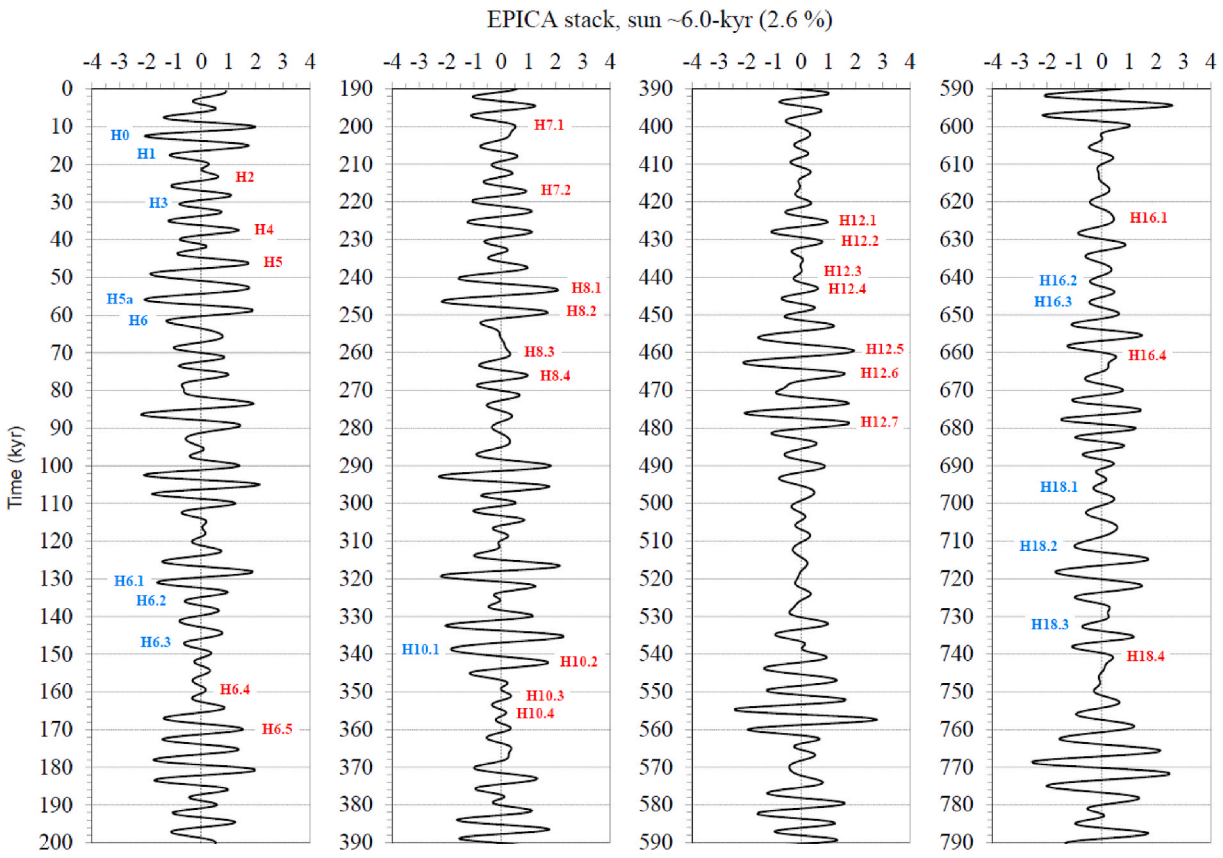

Fig. 7. Time-series panel of the EPICA stack ~6.0-kyr cycle and proposed correlation pattern of the Heinrich and Heinrich-like events of Channell et al. (2012). Light blue label: 'cold-related' Heinrich event; red label: 'warm-related' Heinrich event (see text for discussion). For the first seven Heinrich events, see also Fig. 8. Data standardized (0-mean, 1-std.dev.).

2004). The EPICA stack signal results in a variance of 3.8%. Viaggi (2018) isolates 12–13-kyr periodicity components from global LR04 $\delta^{18}O$ (Lisiecki and Raymo, 2005) and equatorial SST records (Herbert et al., 2010), which is interpreted as a half-precession cycle at 10–12 kyr of equatorial origin owing to the twice-yearly passage of the Sun across the intertropical zone (Berger and Loutre, 1997; Berger et al., 2006). The results of the magnetic susceptibility and particle-size analysis from the Northwestern Chinese Loess Plateau reveal well-defined half-precession cycles during the last interglaciation, and this is interpreted as a direct response to low-latitude forcing through its modulation of the East Asian summer monsoon (Sun and Huang, 2006). Both the polar atmospheric circulation index and the mid- to low-latitude atmospheric circulation index of Mayewski et al. (1997) glaciochemical series display an 11.1-kyr cycle with a stronger power in the latter signal; this is consistent with a possible low-latitude half-precession origin. Wu et al. (2012) have found 12.3–12.6-kyr cycles from South China, Early Triassic rock magnetic cyclostratigraphic record. Cycles expressed by variations in magnetic susceptibility were likely to have resulted from changes in the input of fine-grained detrital magnetite, which in turn may have been driven by half-precession induced changes in monsoon intensity in the equatorial eastern Paleotethys during the Early Triassic by the biannual passage of the Sun across the intertropical zone (Wu et al., 2012). The DCM component-5-6s variability (13 kyr) recorded in Antarctica ice-cores supports the hypothesis of a direct response of equatorial forcing to high latitudes via advective transport (Hagelberg et al., 1994; Turney et al., 2004; Sun and Huang, 2006; Viaggi, 2018). Interestingly, several studies report Late Pleistocene-Holocene worldwide geomagnetic secular variations at sub-Milankovitch frequency bands, including as well a 13.5-kyr cycle (Creer and Tucholka, 1983; Hagee and Olson, 1989; Gogorza et al., 2000). On the other hand, Pestiaux et al. (1988) have found 12.8–13-kyr paleoclimatic oscillations from Late Pleistocene $\delta^{18}O$ Indian Ocean core records, interpreted as 12.4–13 kyr nonlinear oscillator combination tones of primary Milankovitch forcing. Da Silva et al. (2018), by studying Early Devonian hemipelagic carbonate Titanium cyclostratigraphy, found a 10–12-kyr cycle which is interpreted as combination tones of Milankovitch cycles. It is therefore possible that the origin of this cycle is more complex than generally thought.

Sun – New results of the present study indicate that the three EPICA Sun-related cycles (stack signals ~9.7-kyr, ~6.0-kyr and Hallstatt 2.5-kyr), which are recognized for the first time as 800,000-yr-long time-series, cumulatively explain ~4.0% (δD), 2.9% (CO_2) and 6.6% (CH_4) of the total variance (Fig. 10, Table 6). The cumulative mean variance of the stack signals is 4.5%. In terms of individual contribution, the EPICA ~9.7-kyr cycle results in a variance of 1.7% (δD), 1.1% (CO_2) and 2.6% (CH_4). The quantitative impact of the ~6.0-kyr cycle on the Antarctic signals is estimated to be 2.2% (δD), 1.7% (CO_2) and 3.8% (CH_4), and the contribution of the Hallstatt cycle is estimated in 0.05% (δD), 0.1% (CO_2) and 0.2% (CH_4). The fact that Sun-related periodicities are recorded in the Antarctic atmospheric temperature (δD) as well as in the atmospheric content of CO_2 and CH_4 indicates a link between SA, atmospheric temperature and GHGs. These Antarctic evidences of millennial cycles indicate that SA is characterized by long-term dynamics which likely affect the Earth's climate system and atmospheric circulation, considering that the CH_4 content results from changes in wetlands in the tropics and high northern latitudes (Loulergue et al., 2008; Past interglacials working group of PAGES, 2016). However, it should be noted that the cumulative magnitude of the climate responses induced by these frequency bands of solar forcing is limited to just ~4.0% in terms of Antarctic atmospheric temperature (δD) during the last 800,000 years, suggesting a minor role of the SA in the regional

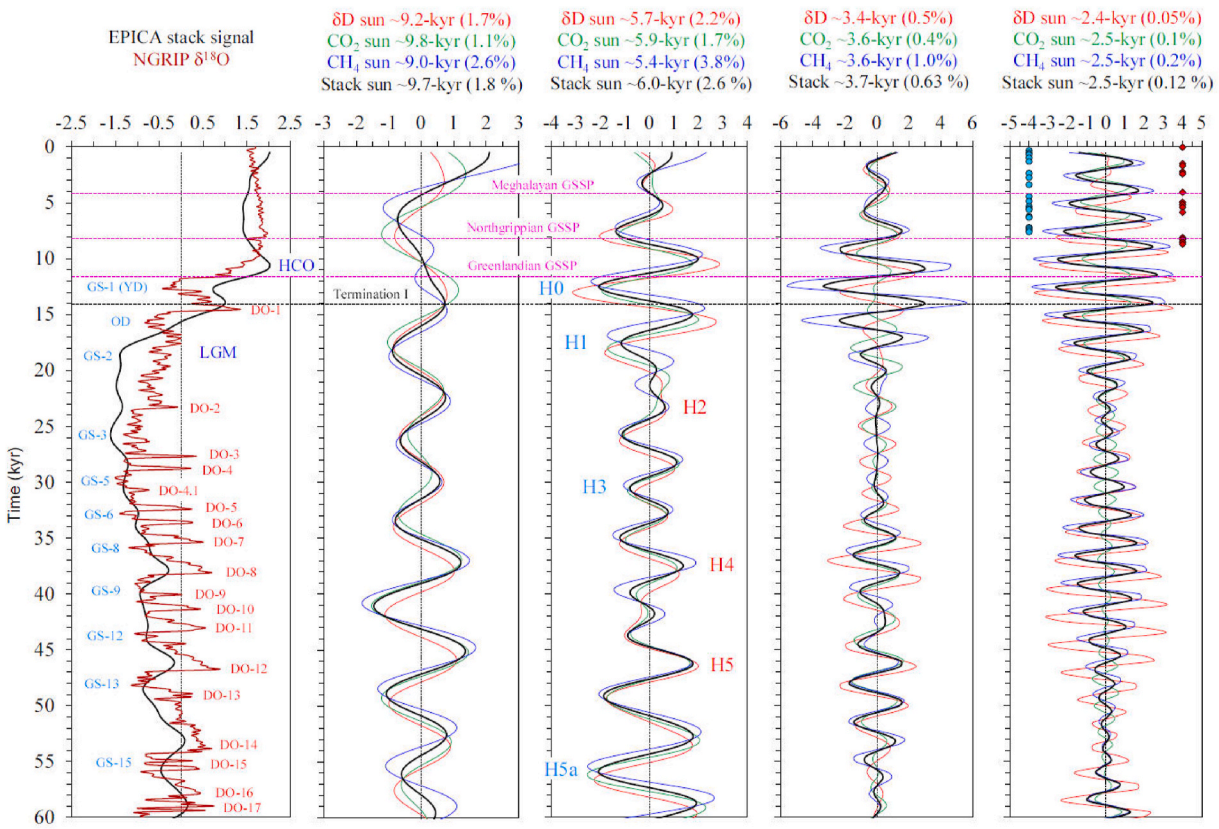

Fig. 8. Time-series panel of the last 60 kyr of EPICA δD, CO_2, CH_4 and stack Sun-related (~9.7-kyr; ~6.0-kyr; ~2.5-kyr) and ~3.7-kyr signals with their approximate correlation with NGRIP $\delta^{18}O$ (NGRIP Community Members, 2007) and North Atlantic glaciological events: Greenland Stadials (GS) from Rasmussen et al. (2014); Dansgaard-Oeschger cycles (DO) from EPICA Community Members (2006); Heinrich events (H) from Channell et al. (2012). YD = Younger Dryas; OD = Oldest Dryas; HCO = Holocene Climatic Optimum; Holocene GSSP boundaries from Walker et al. (2019). Sunspot numbers Grand minima (blue circles) and Grand maxima (red diamonds) centres from Usoskin et al. (2016). Age models: NGRIP (GICC05 adjusted to BP); EPICA (AICC2012). Data standardized (0-mean, 1-std.dev.). EPICA original data from Past interglacials working group of PAGES (2016).

budget of Earth's climate forcing.

Unclear ~3.6-kyr cycle – Finally, a 0.4–1.0% DCM signal variance is referred to as a 3.4–3.6-kyr cycle of unclear origin, which is not well known in literature. The mean variance of the stack signal is 0.6%. This cycle is close to a geomagnetic secular variation of 3.0–3.8 kyr (Creer and Tucholka, 1983; Hagee and Olson, 1989; Gogorza et al., 2000; Wu et al., 2012), as well as similar to a 2.9–3.1 kyr beat of nonlinear Milankovitch oscillator (Pestiaux et al., 1988), but it appears to be absent from solar proxies (Fig. 4).

3.6. Lead-lag patterns of Antarctic signals by forcing

The phase relationships determined by cross-spectral analysis of the δD vs. CO_2 and CH_4 standardized components are shown in Table 7 by forcing. The mid-term oscillation phase analysis is based on peak detection and delta age average (Fig. 9). As the original EPICA records are all recalibrated on the AICC2012 age model (Bazin et al., 2013; Past interglacials working group of PAGES, 2016), there should be negligible differences between the records in the age model. The coherency of the signals is quite variable, but an average decreasing trend towards the short periodicities is observed. In particular, the sub-Milankovitch frequencies exhibit a very low coherency.

Even the phase shift is diversified with a general delayed pattern on both mid-term oscillation and orbital frequency bands (with an exception in the obliquity CH_4 signal). On the contrary, the sub-Milankovitch bands (from ~9.3 kyr to 2.5 kyr) exhibit low coherency and unstable phase patterns, resulting in an average leading pattern (again, with the exception of 6.3-kyr CH_4 signal). The phase relationships contain useful information to address the causal mechanisms at the origin of paleoclimatic responses. In the following lines the possible mechanisms are discussed with a special focus on the Sun-related signals.

A lagging GHGs pattern of astronomical climate responses is in general agreement with reports by many authors (Imbrie et al., 1993; Shackleton, 2000; Lisiecki and Raymo, 2005; Tziperman et al., 2006; Hansen et al., 2007; Schneider et al., 2013; Past interglacials working group of PAGES, 2016; Viaggi, 2018), and suggest a climate system affected by feedback processes that are induced by initial temperature change on the Earth's surface, which are even the most likely mechanisms behind non-linearities in the climate (Archer et al., 2004; Rial et al., 2004; Lisiecki and Raymo, 2007; Brovkin et al., 2007; Hansen et al., 2007; Kohler et al., 2010; Viaggi, 2018). The main positive feedback mechanisms, such as the CO_2 exchange between the ocean and the atmosphere (Hain et al., 2010), the water-vapour feedback (Kohler et al., 2010), the GHG release from permafrost peat bogs and from hydrates (Tarnocai et al., 2009) and the surface albedo feedback (Willeit and Ganopolski, 2018), lead to an amplified climate response to primary forcing.

Recent studies shed new light on the link between SA and Earth's climate, although there are substantial uncertainties in the magnitude and mechanisms of Sun-climate interactions (Shindell et al., 2020). Almost all the incoming TSI at the top of the Earth's atmosphere is in the ultraviolet, visible and infrared regions, and approximately 50% of this radiation penetrates the atmosphere and is absorbed at the surface (Gray et al., 2010). The direct absorption of TSI by oceans is likely to be significant because of the large oceanic heat capacity, which can 'integrate' long-term variations in heat input. Further, some of the radiation is

Table 6
Complete suite of EPICA δD, CO_2, and CH_4 signals by forcing and their quantitative impact (% variance) on the Pleistocene climate system. The stacks by forcing are calculated as weighted mean by variance of the δD, CO_2, and CH_4 signals (details in Additional file 1). The frequency peaks are the most significant above a 99.9% critical limit.

Forcing	Record	Period (kyr)	Variance (%)
Mid-term oscillation	δD	–	2.0
	CO_2	–	7.7
	CH_4	–	3.5
	Stack	–	4.4
Obliquity mod. cycle	δD	157	3.7
	CO_2	240	5.8
	CH_4	239	2.5
	Stack	184	4.0
Short eccentricity	δD	93	50.5
	CO_2	96	58.9
	CH_4	96	45.5
	Stack	95	51.6
Obliquity	δD	41	23.4
	CO_2	45	11.9
	CH_4	43	21.7
	Stack	42	19.0
Precession	δD	23	9.3
	CO_2	23	5.9
	CH_4	21	9.9
	Stack	22	8.4
Half-precession	δD	13	3.5
	CO_2	13	2.5
	CH_4	13	5.3
	Stack	13	3.8
Sun	δD	9.2	1.7
	CO_2	9.8	1.1
	CH_4	9.0	2.6
	Stack	9.7	1.8
Sun	δD	5.7	2.2
	CO_2	5.9	1.7
	CH_4	5.4	3.8
	Stack	6.0	2.6
Unclear	δD	3.4	0.5
	CO_2	3.6	0.4
	CH_4	3.6	1.0
	Stack	3.7	0.6
Sun	δD	2.4	0.05
	CO_2	2.5	0.10
	CH_4	2.5	0.20
	Stack	2.5	0.12

absorbed in the atmosphere, primarily by tropospheric water vapour in several wavelength bands and by stratospheric ozone in the ultraviolet region, the latter having a non-negligible effect (Haigh et al., 2005; Gray et al., 2010; Shang et al., 2013). The direct effect of ultraviolet irradiance is amplified by an important feedback mechanism involving new ozone production, which is an additional source of heating and temperature gradients (Gray et al., 2009; Shang et al., 2013). Thus, solar-induced variations in the ozone layer can directly affect the radiative balance of the stratosphere, with indirect effects on tropospheric circulation leading to changes in the zonal wind and planetary wave–mean flow interactions, affecting Earth's regional climate (Haigh et al., 2005; Claud et al., 2008; Gray et al., 2010). These tropospheric changes, which are partly due to stratosphere-troposphere coupling by the 'top-down' mechanism, appear to work in the same direction as the 'bottom-up' mechanisms based on solar heating of the sea surface and dynamically coupled sea-air interaction (Meehl et al., 2008). These changes could be additive to produce the response in the climate system to solar forcing (Rind et al., 2008). The 'bottom-up' mechanism dominate the tropical response to solar forcing, whereas both 'top-down' and 'bottom-up' mechanisms can be important at mid-to-high latitudes, especially during the boreal cold-season. However, their relative importance remains unclear (Shindell et al., 2020). Another Sun-related physical mechanism concerns a cosmic ray-cloud cover feedback on climate (Svensmark and Friis-Christensen, 1997). Clouds play an important part in establishing the heat and radiation budgets of the atmosphere. They reflect about 15% of the incoming solar radiation directly back to space, but they also trap infrared radiation acting in a similar way to greenhouse gases (Haigh 2011). According to Svensmark and Friis-Christensen (1997) the cosmic ray flux, modulated by 11-yr solar activity, by increasing the number of ions in the atmosphere leading to enhanced condensation of water vapour and cloud droplet formation, may modify global cloud cover and global surface temperature. The feedback is larger at higher latitudes in agreement with the shielding effect of the Earth's magnetic field on high-energy charged particles. However, this hypothesis is not confirmed by the work of Sun and Bradley (2002). The cosmic ray-cloud cover feedback mechanisms are physically plausible but evidence for a significant impact remains elusive (Haigh 2011). Hypothesizing similar processes on Sun-related millennial time scales, these mechanisms should lead to an advance of the temperature on GHGs, in contrast to the EPICA observations. Interestingly, Viaggi (2018) finds that the exponential growth of the Plio-Pleistocene $\delta^{18}O$ orbitals variance towards the Late Pleistocene is a function of the global increasing trend of ice-volume with an increasing rate as being related to the period, from half-precession to eccentricity. This observation appears to indicate that the sensitivity of orbital responses to feedback lagged processes is decreasing towards short-period forcing. Thus, the suborbital and Sun-related cycles may be less sensitive to the delayed mechanisms of feedbacks and be more influenced by other processes, like ocean heat inertia. The large heat inertia of the Southern Ocean (Stocker and Johnsen, 2003) could overlap a delayed temperature response, leading to an unstable low coherency phase pattern at the scale of suborbital bands.

4. Conclusions

The main conclusions of this research can be summarized as follows:

1) The quantitative impact of the three EPICA Sun-related cycles (unnamed ~9.7-kyr, unnamed ~6.0-kyr and Hallstatt 2.5-kyr) cumulatively explain the total variance of ~4.0% (δD), 2.9% (CO_2) and 6.6% (CH_4), demonstrating a minor role of the SA in the regional budget of Earth's climate forcing.
2) The occurrence in solar proxies of a ~5.7-kyr SA cycle and ~5.8-kyr TSI cycle support a Sun-related origin of the EPICA stack ~6.0-kyr oscillation. According to the recurrence analysis of Heinrich events (6.03 ± 1.4 kyr) and their correlation with EPICA ~6.0-kyr cycle, it is proposed that this band of SA be named the 'Heinrich-Bond cycle' because Heinrich (1988) and Bond et al. (1993) first noted the occurrence of IRD layers linked to the SST from North Atlantic sediments. The quantitative impact of the Heinrich-Bond cycle on the Antarctic signals is estimated as 2.2% (δD), 1.7% (CO_2) and 3.8% (CH_4). Some Heinrich and Heinrich-like events would appear to be related to the heating phases of the ~6.0-kyr cycle, suggesting a destabilization of the ice-sheet for surface heating and meltwater streams ('warm-related' Heinrich event), along with the traditional notion of 'cold-related' Heinrich events.
3) The quantitative impact of the ~2.5-kyr Hallstatt cycle on the Antarctic signals is estimated as 0.05% (δD), 0.1% (CO_2) and 0.2% (CH_4). This cycle is found in a number of solar proxies, geomagnetic secular variations, paleoclimatic oscillations, nonlinear harmonics, or combination tones of primary Milankovitch cycles as well as resonant planetary beats, indicating an apparent 'multi-forcing' origin possibly related to PBH.
4) A cycle of ~3.6 kyr of unclear origin, which is little known in literature, has been detected in EPICA records, and results in a variance of 0.5% (δD), 0.4% (CO_2), and 1.0% (CH_4). This cycle is close even to a geomagnetic secular variations of 3.0–3.8 kyr, as well as similar to the 2.9–3.1-kyr beat of the nonlinear Milankovitch oscillator, but it appears to be absent from solar proxies. Therefore, this cycle does

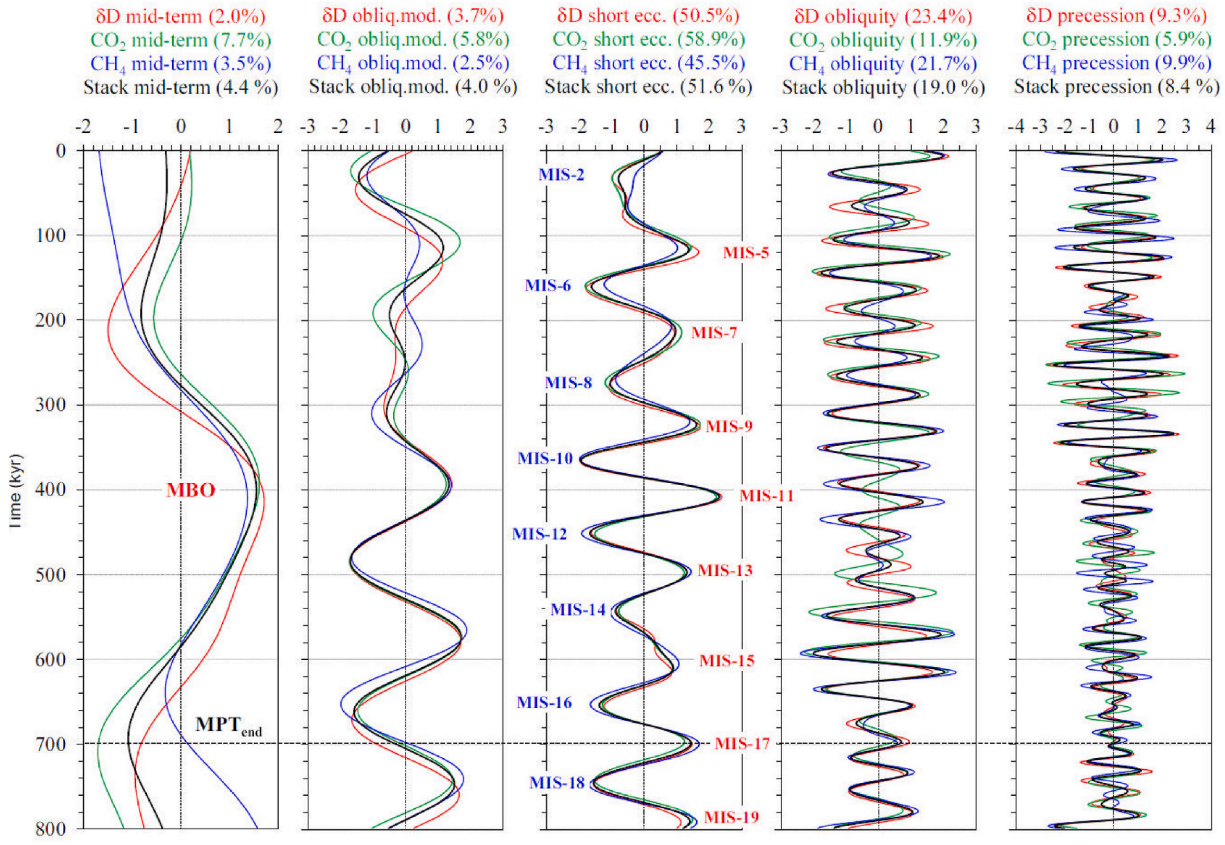

Fig. 9. Time-series panel of EPICA δD, CO_2, CH_4 and stack signals of mid-term and orbital components with their magnitude as % variance. Mid-Brunhes oscillation (MBO) (Viaggi, 2018). MIS from Lisiecki and Raymo (2005). Data standardized (0-mean, 1-std.dev.). EPICA original data from Past interglacials working group of PAGES (2016).

not seem to be Sun-related, although a gravitational origin cannot be ruled out.

5) The fact that Sun-related periodicities are recorded in the Antarctic atmospheric temperature (δD) as well as in the atmospheric content of CO_2 and CH_4 indicates a link between the SA, atmospheric temperature and GHGs with millennial-scale dynamics affecting the Earth's climate system, albeit with a low quantitative impact.
6) An EPICA Mid-term oscillation named MBO showing a mild warming phase centred at ~400 kyr ago results in a variance of 2.0% (δD), 7.7% (CO_2) and 3.5% (CH_4), and correlates to the wide swing of the LR04 $\delta^{18}O$ long-term component depletion at ~400–300 kyr ago. The MIS-11 could be an astronomical event boosted by this GHGs mid-term recovery, although some doubts about its effectiveness concern its low quantitative impact.
7) The quantitative impact of the EPICA astronomical components consistently reflects the post-MPT nature of the records in which the short eccentricity results in most of the variance being estimated at 50.5% (δD), 58.9% (CO_2) and 45.5% (CH_4), whereas the obliquity accounts for 23.4% (δD), 11.9% (CO_2) and 21.7% (CH_4), respectively. The precession has a variance of 9.3% (δD), 5.9% (CO_2) and 9.9% (CH_4). A small variance of 3.7% (δD), 5.8% (CO_2) and 2.5% (CH_4) is related to the obliquity amplitude modulation cycles.
8) The EPICA half-precession components have variances of 3.5% (δD), 2.5% (CO_2) and 5.3% (CH_4), and support the hypothesis of a direct response of intertropical forcing to high latitudes via advective transport. However, the occurrence of a similar periodicity in worldwide geomagnetic secular variations as well as nonlinear oscillator combination tones of primary Milankovitch forcing might suggest that the origin of this cycle is more complex than generally thought.
9) The EPICA phase relationships generally show a delayed pattern between the carbon-GHGs and the δD atmospheric temperature both on mid-term and orbital bands, suggesting a climate system affected by feedback processes and delay mechanisms after temperature change. On the contrary, the sub-Milankovitch bands show low coherency and unstable lead/lag patterns. The large heat inertia of the Southern Ocean could superimpose a delayed temperature response on a suborbital band less sensitive to the carbon-GHGs feedback mechanisms, leading to an unstable low coherence phase pattern.

PBH is an intriguing hypothesis that has the potential to unify the apparent contradictions of 'multi-forcing' suborbital cycles. However, it requires in-depth studies related to the understanding of the physical processes that would regulate the electromagnetic activity of the Sun, as well as the possible direct and indirect effects on the Earth, considering especially the very low magnitude of the planetary gravitational beat. The recent discoveries by Zharkova et al. (2019) appear to be going in the right direction. Beyond the Milankovitch theory, evidence is emerging of a multiple forcing cosmoclimatic system with stochastic interactions between external (gravitational resonances, orbitals, SA) and Earth's internal (geodynamics, atmosphere composition, feedback mechanisms) climate components, each having a strong difference in the relative quantitative impact on Earth's climate.

Data availability statement

Supplementary information files are included in this published article.

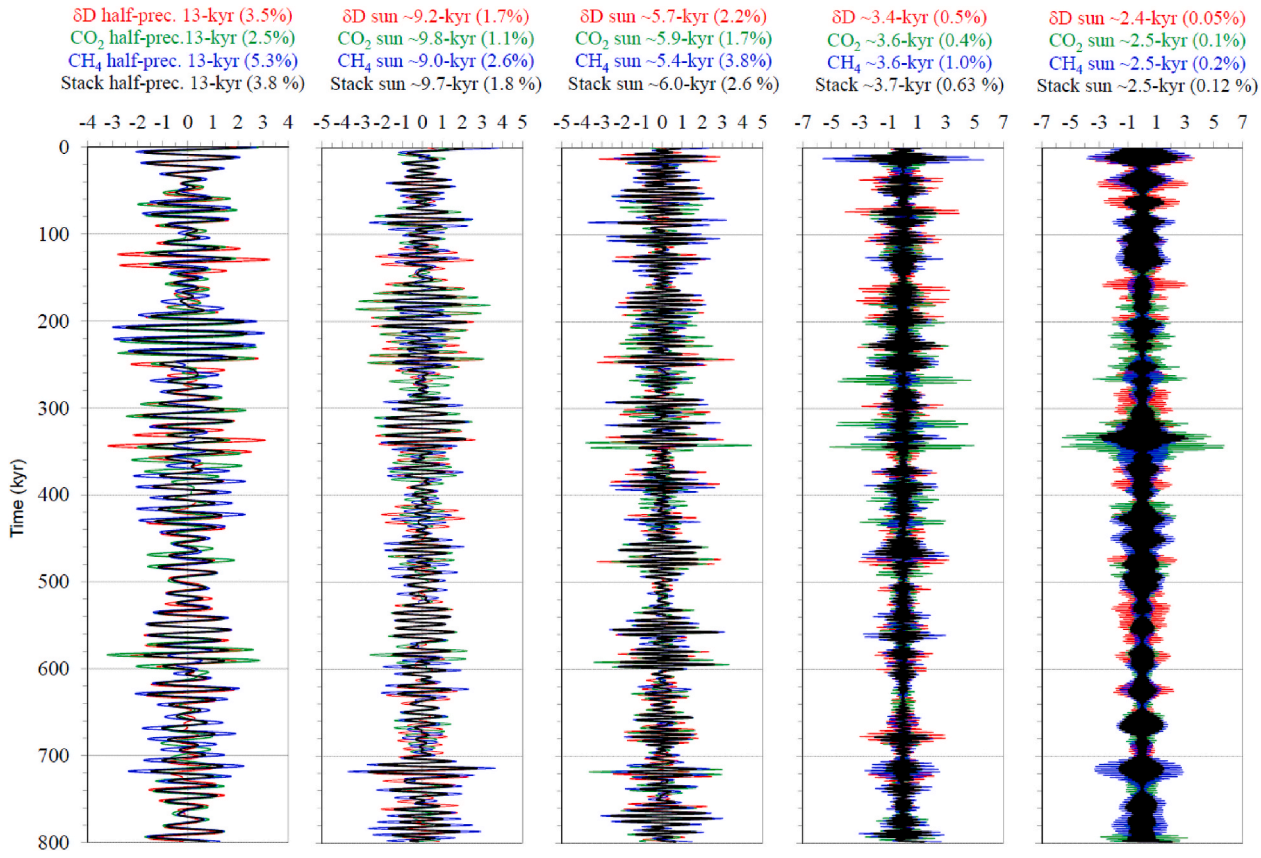

Fig. 10. Time-series panel of EPICA δD, CO_2, CH_4 and stack sub-Milankovitch signals with their magnitude as % variance. Data standardized (0-mean, 1-std.dev.). EPICA original data from Past interglacials working group of PAGES (2016).

Table 7
Results of the cross-spectral analysis among the EPICA δD vs. CO_2 and CH_4 standardized (mean = 0, standard deviation = 1) SSA-components by forcing. Mid-term oscillation analysis by peak detection (delta age mean). Orbitals (Hann window); suborbitals (15-points smoothed Hann window).

Forcing	Signal		Cross-spectrum freq. (kyr^{-1})	Cross-spectrum period (kyr)	Coherency	Phase shift (Deg, kyr)		
Mid-term oscillation[1]	δD vs.	CO_2		–	–	–	−21.8	CO_2 lags δD
		CH_4	–	–	–	–	−51.3	CH_4 lags δD
Obliquity mod. cycle	δD vs.	CO_2	0.00625	160.0	0.98	−21.9	−9.7	CO_2 lags δD
		CH_4	0.00625	160.0	0.97	−39.7	−17.6	CH_4 lags δD
Short Eccentricity	δD vs.	CO_2	0.01	100.0	0.98	−7.4	−2.06	CO_2 lags δD
		CH_4	0.01	100.0	0.96	−13.8	−3.83	CH_4 lags δD
Obliquity	δD vs.	CO_2	0.025	40.0	0.45	−25.9	−2.88	CO_2 lags δD
		CH_4	0.025	40.0	0.88	7.7	0.86	CH_4 leads δD
Precession	δD vs.	CO_2	0.0425	23.5	0.95	−28.1	−1.84	CO_2 lags δD
		CH_4	0.0425	23.5	0.64	34.3	2.24	CH_4 leads δD
Half-precession	δD vs.	CO_2	0.08125	12.3	0.53	−1.3	−0.044	CO_2 lags δD
		CH_4	0.08000	12.5	0.43	−19.1	−0.663	CH_4 lags δD
Sun	δD vs.	CO_2	0.11125	9.0	0.22	18.2	0.454	CO_2 leads δD
		CH_4	0.10500	9.5	0.15	8.8	0.233	CH_4 leads δD
Sun	δD vs.	CO_2	0.15250	6.6	0.74	1.2	0.022	CO_2 leads δD
		CH_4	0.15750	6.3	0.58	−16.6	−0.293	CH_4 lags δD
Unclear	δD vs.	CO_2	0.28000	3.6	0.22	27.8	0.276	CO_2 leads δD
		CH_4	0.30625	3.3	0.28	37.8	0.343	CH_4 leads δD
Sun	δD vs.	CO_2	0.39375	2.5	0.20	30.2	0.213	CO_2 leads δD
		CH_4	0.40500	2.5	0.18	7.3	0.050	CH_4 leads δD

Declaration of competing interest

The authors declare that they have no known competing financial interests or personal relationships that could have appeared to influence the work reported in this paper.

Acknowledgements

The author is grateful to Gian Battista Vai for the useful suggestions and enhancements to the paper.

Abbreviations

comp: component

DCM	δD, CO_2, and CH_4 EPICA records
DO	Dansgaard-Oeschger cycle
ENSO	El Nino/Southern Oscillation
EPICA	European Project for Ice Coring in Antarctica
FFS	Fourier frequency spectrum
GHG	green-house gas
GISP2	Greenland Ice Sheet Project 2
GS	Greenland Stadials
H	Heinrich event
IRD	ice-rafted debris
MBO	Mid-Brunhes oscillation
MIS	marine isotope stage
MPT	Mid-Pleistocene transition
NGRIP	North Greenland Ice Core Project
PBH	planetary beat hypothesis
PGF	planetary gravitational forcing
SA	solar activity
SIM	solar inertial motion
SSA	singular spectrum analysis
SST	sea surface temperature
subcomp	subcomponent
TISA	time-integral squared amplitude
TSI	total solar irradiance

Appendix A. Supplementary data

Supplementary data to this article can be found online at https://doi.org/10.1016/j.qsa.2021.100037.

References

Abreu, J.A., Beer, J., Ferriz-Mas, A., McCracken, K.G., Steinhilber, F., 2012. Is there a planetary influence on solar activity? Astron. Astrophys. 548, A88. https://doi.org/10.1051/0004-6361/201219997.

Alley, R.B., 1998. Icing the north Atlantic. Nature 392 (26 March 1998), 335–337.

Alley, R.B., Clark, P.U., Keigwin, L.D., Webb, R.S., 1999. Making sense of millennial-scale climate change. In: Clark, P.U., et al. (Eds.), Mechanisms of Global Climate Change at Millennial Time Scales: Am. Geophys. Union Geophys, vol. 112, pp. 385–394. Monogr.

Andrews, J.T., Jennings, A.E., Kerwin, M., Kirby, M., Manley, W., Miller, G.H., Bond, G., MacLean, B., 1995. A heinrich-Iike event, H-0 (DC-O): source(s) for detrital carbonate in the north Atlantic during the Younger Dryas chronozone. Paleoceanography 10 (No. 5), 943–952. October 1995.

Archer, D., Martin, P., Buffett, B., Brovkin, V., Rahmstorf, S., Ganopolski, A., 2004. The importance of ocean temperature to global biogeochemistry. Earth Planet Sci. Lett. 222, 333–348. https://doi.org/10.1016/j.epsl.2004.03.011.

Bard, E., Frank, M., 2006. Climate change and solar variability: what's new under the sun? Earth Planet Sci. Lett. 248, 1–14. https://doi.org/10.1016/j.epsl.2006.06.016.

Bazin, L., Landais, A., Lemieux-Dudon, B., Toyé Mahamadou Kele, H., Veres, D., Parrenin, F., Martinerie, P., Ritz, C., Capron, E., Lipenkov, V., Loutre, M.-F., Raynaud, D., Vinther, B., Svensson, A., Rasmussen, S.O., Severi, M., Blunier, T., Leuenberger, M., Fischer, H., Masson-Delmotte, V., Chappellaz, J., Wolff, E., 2013. An optimized multi-proxy, multi-site Antarctic ice and gas orbital chronology (AICC2012): 120–800 ka. Clim. Past 9, 1715–1731. https://doi.org/10.5194/cp-9-1715-2013.

Bereiter, B., Eggleston, S., Schmitt, J., Nehrbass-Ahles, C., Stocker, T.F., Fischer, H., Kipfstuhl, S., Chappellaz, J., 2015. Revision of the EPICA Dome CCO_2 record from 800 to 600 kyr before present. Geophys. Res. Lett. 42, 1–8. https://doi.org/10.1002/2014GL061957.

Berger, A., 1988. Milankovitch theory and climate. Rev. Geophys. 26 (4), 624–657. November 1988.

Berger, A., Loutre, M.F., 1997. Long-term variations in insolation and their effects on climate, the LLN experiments. Surv. Geophys. 18, 147–161.

Berger, A., Yin, Q., 2012. Modeling the interglacials of the last 1 million years. In: Berger, et al. (Eds.), Climate Change: Inferences from Paleoclimate and Regional Aspects. Springer-Verlag, Wien.

Berger, A., Loutre, M.F., Mélice, J.L., 2006. Equatorial insolation: from precession harmonics to eccentricity frequencies. Clim. Past Discuss 2, 519–533. https://doi.org/10.5194/cp-2-131-2006.

Berger, A., Yin, Q.Z., Herold, N., 2012. MIS-11 and MIS-19, analogs of our Holocene interglacial. Hamburg 3rd Int. Conf. On Earth Syst.Model.. https://meetingorganizer.copernicus.org/3ICESM/3ICESM-11.pdf.

Bond, G., Broecker, W., Johnsentt, S., McManus, J., Labeyrie, L., Jean Jouzel, J., Bonani, G., 1993. Correlations between climate records from North Atlantic sediments and Greenland ice. Nature 365, 143–147, 9 September 1993.

Bond, G., Showers, W., Cheseby, M., Lotti, R., Almasi, P., deMenocal, P., Priore, P., Cullen, H., Hajdas, I., Bonani, G., 1997. A pervasive millennial-scale cycle in North Atlantic Holocene and glacial climates. Science 278, 1257–1266, 14 November 1997.

Bond, G., Kromer, B., Beer, J., Muscheler, R., Evans, M.N., Showers, W., Hoffmam, S., Lotti-Bond, R., Hajdas, I., Bonani, G., 2001. Persistent solar influence on North Atlantic climate uring the Holocene. Science 294, 2130–2136, 7 December 2001.

Boulila, S., Galbrun, B., Miller, K.G., Pekar, S.F., Browning, J.V., Laskar, J., Wright, J.D., 2011. On the origin of Cenozoic and Mesozoic "third-order" eustatic sequences. Earth Sci. Rev. 109, 94–112.

Brovkin, V., Ganopolski, A., Archer, D., Rahmstorf, S., 2007. Lowering of glacial atmospheric CO_2 in response to changes in oceanic circulation and marine biogeochemistry. Paleoceanography 22, PA4202. https://doi.org/10.1029/2006PA001380.

Cauquoin, A., Raisbeck, G.M., Jouzel, J., Bard, E., ASTER Team, 2014. No evidence for planetary influence on solar activity 330,000 years ago. Astron. Astrophys. 561, A132. https://doi.org/10.1051/0004-6361/201322879.

Channell, J.E.T., Xuan, C., Hodell, D.A., 2009. Stacking paleointensity and oxygen isotope data for the last 1.5 Myrs (PISO-1500). Earth Planet Sci. Lett. 283, 14–23.

Channell, J.E.T., Hodell, D.A., Romero, O., Hillaire-Marcel, C., de Vernal, A., Stoner, J.S., Mazaud, A., Röhl, U., 2012. A 750-kyr detrital-layer stratigraphy for the north Atlantic (IODP sites U1302–U1303, Orphan Knoll, Labrador Sea). Earth Planet Sci. Lett. 317–318, 218–230. https://doi.org/10.1016/j.epsl.2011.11.029.

Charvátová, I., 2000. Can origin of the 2400-year cycle of solar activity be caused by solar inertial motion? Ann. Geophys. 18, 399–405.

Charvátová, I., Hejda, P., 2014. - Responses of the basic cycles of 178.7 and 2402 yr in solar–terrestrial phenomena during the Holocene. In: Mörner, N.-A., Tattersall, R., Solheim, J.-E. (Eds.), Pattern in Solar Variability, Their Planetary Origin and Terrestrial Impacts. Pattern Recognit. In Phys., Special Issue, vol. 2, pp. 21–26. https://doi.org/10.5194/prp-2-21-2014, 2014, Copernicus Publications.

Claud, C., Cagnazzo, C., Keckhut, P., 2008. The effect of the 11-year solar cycle on the temperature in the lower stratosphere. J. Atmos. Sol. Terr. Phys. 70, 2031–2040. https://doi.org/10.1016/j.jastp.2008.07.010.

Clemens, S.C., 2005. Millennial-band climate spectrum resolved and linked to centennial-scale solar cycles. Quat. Sci. Rev. 24, 521–531. https://doi.org/10.1016/j.quascirev.2004.10.015.

Creer, K.M., Tucholka, P., 1983. On the current state of lake sediment palaeomagnetic research. Geophys. JR Astr. Soc. 74, 223–238.

Da Silva, A.C., Dekkers, M.J., De Vleeschouwer, D., Hladil, J., Chadimova, L., Slavík, L., Hilgen, F.J., 2018. Millennial-scale climate changes manifest Milankovitch combination tones and Hallstatt solar cycles in the Devonian greenhouse world. Geol. 47, 1–4. https://doi.org/10.1130/G45511.1.

De Michelis, P., Tozzi, R., Meloni, A., 2005. Geomagnetic jerks: observation and theoretical modeling. Mem. SA It 76, 957–960.

Dergachev, V.A., 2004. Manifestation of the long-term solar cyclicity in climate archives over 10 millennia. In: Stepanov, A.V., Benevolenskaya (Eds.).

Elrick, M., Hinnov, L.A., 2007. Millennial-scale paleoclimate cycles recorded in widespread Paleozoic deeper water rhythmites of North America. Palaeogeogr. Palaeoclimatol. Palaeoecol. 243, 348–372. https://doi.org/10.1016/j.palaeo.2006.08.008.

Elsner, J.B., Tsonis, A.A., 1996. Singular Spectrum Analysis: a New Tool in Time Series Analysis, 1996. Springer.

Engels, S., van Geel, B., 2012. The effects of changing solar activity on climate: contributions from palaeoclimatological studies. J. Space Weather Space Clim. 2, A09. https://doi.org/10.1051/swsc/2012009.

EPICA Community Members, 2006. One-to-one coupling of glacial climate variability in Greenland and Antarctica. Nature 444, 195–198. https://doi.org/10.1038/nature0530, 9 November 2006.

Franco, D.R., Hinnov, L.A., 2012. Anisotropy of magnetic susceptibility and sedimentary cycle data from Permo-Carboniferous rhythmites (ParanàBasin, Brazil): a multiple proxy record of astronomical and millennial scale palaeoclimate change in a glacial setting. In: Jovane, L., Herrero-Bervera, E., Hinnov, L.A., Housen, B.A. (Eds.), Magnetic Methods and the Timing of Geological Processes. Geol. Soc., London, Special Publications, vol. 373. https://doi.org/10.1144/SP373.11.

Franco, D.R., Hinnov, L.A., Ernesto, M., 2012. Millennial-scale climate cycles in Permian–Carboniferous rhythmites: permanent feature throughout geologic time? Geol. 40 (1), 19–22. https://doi.org/10.1130/G32338.1.

Georgieva, K., Kirov, B., Nagovitsyn, YuA., 2013. Long-term variations of solar magnetic fields derived from geomagnetic data. Geomagn.and Aeron., December 53 (7), 852–856. https://link.springer.com/article/10.1134/S0016793213070062.

Ghil, M., Allen, R.M., Dettinger, M.D., Ide, K., Kondrashov, D., Mann, M.E., Robertson, A., Saunders, A., Tian, Y., Varadi, F., Yiou, P., 2002. Advanced spectral methods for climatic time series. Rev. Geophys. 40 (1), 3. https://doi.org/10.1029/2001RG000092, 1–3.41.

Gogorza, C.S.G., Sinito, A.M., Vilas, J.F., Creer, K.M., Nunez, H., 2000. Geomagnetic secular variations over the last 6500 years as recorded by sediments from the lakes of south Argentina. Geophys. J. Int. 143, 787–798.

Gray, L.J., Rumbold, S.T., Shine, K.P., 2009. Stratospheric temperature and radiative forcing response to 11-year solar cycle changes in irradiance and ozone. J. Atmos. Sci. 66, 2402–2417. https://doi.org/10.1175/2009JAS2866.1.

Gray, L.J., Beer, J., Geller, M., Haigh, J.D., Lockwood, M., Matthes, K., Cubasch, U., Fleitmann, D., Harrison, G., Hood, L., Luterbacher, J., Meehl, G.A., Shindell, D., van Geel, B., WhiteW, 2010. Solar influences on climate. Rev. Geophys. 48, RG4001. https://doi.org/10.1029/2009RG000282.

Hagee, V.L., Olson, P., 1989. An analysis of paleomagnetic secular variation in the Holocene. Phys. Earth Planet. In. 56, 266–284.

Hagelberg, T.K., Bond, G., deMenocal, P., 1994. Milankovitch band forcing of sub-Milankovitch climate variability during the Pleistocene. Paleoceanography 9 (4), 545–558. https://doi.org/10.1029/94PA00443.
Haigh, J.D., Blackburn, M., Day, R., 2005. The response of tropospheric circulation to perturbations in lower-stratospheric temperature. J. Clim. 18, 3672–3685 (Am. Meteorol. Soc).
Hain, M.P., Sigman, D.M., Haug, G.H., 2010. Carbon dioxide effects of Antarctic stratification, North Atlantic Intermediate Water formation, and subantarctic nutrient drawdown during the last ice age: diagnosis and synthesis in a geochemical box model. Global Biogeochem. Cycles 24 (GB4023), 1–19. https://doi.org/10.1029/2010GB003790.
Hansen, J., Sato, M., Kharecha, P., Russell, G., Lea, D.W., Siddall, M., 2007. Climate change and trace gases. Phil Trans R Soc A 365, 1925–1954. https://doi.org/10.1098/rsta.2007.2052.
Harzhauser, M., Mandic, O., Kern, A.K., Piller, W.E., Neubauer, T.A., Albrecht, C., Wilke, T., 2013. Explosive demographic expansion by dreissenid bivalves as a possible result of astronomical forcing. Biogeosciences 10, 8423–8431. https://doi.org/10.5194/bg-10-8423-2013.
Hassani, H., 2007. Singular spectrum analysis: methodology and comparison. J. Data Sci. 5, 239–257.
Heinrich, H., 1988. Origin and consequences of cyclic ice rafting in the Northeast Atlantic Ocean during the past 130,000 years. Quat.Res. 29, 142–152.
Herbert, T.D., Peterson, L.C., Lawrence, K.T., Liu, Z., 2010. Tropical ocean temperatures over the past 3.5 million years. Science 328, 1530–1534. https://doi.org/10.1126/science.1185435.
Hodell, D.A., Channell, J.E.T., Curtis, J.H., Romero, O.E., Rohl, U., 2008. Onset of "Hudson strait'' heinrich events in the eastern North Atlantic at the end of the middle Pleistocene transition (~640 ka)? Paleoceanography 23, PA4218. https://doi.org/10.1029/2008PA001591.
Holm, S., 2014. On the alleged coherence between the global temperature and the sun's movement. J. Atmos. Sol. Terr. Phys. 1–10. April 2014.
Imbrie, J., Boyle, E., Clemens, S., Duffy, A., Howard, W., Kukla, G., Kutzbach, J., Martinson, D.G., McIntyre, A., Mix, A.C., Molfino, B., Morley, J.J., Peterson, L.C., Pisias, N.G., Prell, W.L., Raymo, M.E., Shackleton, N.J., Toggweiler, J.R., 1992. On the structure and origin of major glaciation cycles 1. linear responses to milankovitch forcing. Paleoceanography 7 (6), 701–738.
Imbrie, J., Berger, A., Boyle, E.A., Clemens, S.C., Duffy, A., Howard, W.R., Kukla, G., Kutzbach, J., Martinson, D.G., Mcintyre, A., Mix, A.C., Molfino, B., Morley, J.J., Peterson, L.C., Pisias, N.G., Prell, W.L., Raymo, M.E., Shackleton, N.J., Toggweile, J. R., 1993. On the structure and origin of major glaciation cycles 2. The 100,000-year cycle. Paleoceanography 8 (6), 699–735.
Jicha, B.R., Scholl, D.W., Rea, D.K., 2009. Circum-Pacific arc flare-ups and global cooling near the Eocene Oligocene boundary. Geol. 37 (4), 303–306. https://doi.org/10.1130/G25392A.1.
Jouzel, J., et al., 1997. Validity of the temperature reconstruction from water isotopes in ice cores. J. Geophys. Res. 102 (C12), 26 ,471–26,487.
Jouzel, J., et al., 2007. Orbital and millennial Antarctic climate variability over the past 800,000 years. Science 317, 793–796. https://doi.org/10.1126/science.1141038.
Kern, A.K., Harzhauser, M., Piller, W.E., Mandic, O., Soliman, A., 2012. Strong evidence for the influence of solar cycles on a Late Miocene lake system revealed by biotic and abiotic proxies. Palaeogeogr. Palaeoclimatol. Palaeoecol. 329–330, 124–136. https://doi.org/10.1016/j.palaeo.2012.02.023.
Kohler, P., Bintanja, R., Fischer, H., Joos, F., Knutti, R., Lohmann, G., Masson-Delmotte, V., 2010. What caused Earth's temperature variations during the last 800,000 years? Data-based evidence on radiative forcing and constraints on climate sensitivity. Quat. Sci. Rev. 29, 129–145. https://doi.org/10.1016/j.quascirev.2009.09.026.
Kominz, M., Pisias, N., 1979. Pleistocene climate: deterministic or stochastic? Science 204, 171–173. https://doi.org/10.1126/science.204.4389.171 lssue 4389.
Laskar, J., Fienga, A., Gastineau, M., Manche, H., 2011. La2010: a new orbital solution for the long-term motion of the Earth. Astron. Astrophys. 532, A89. https://doi.org/10.1051/0004-6361/201116836.
Lisiecki, L.E., Raymo, M.E., 2005. A Pliocene-Pleistocene stack of 57 globally distributed benthic δ18O records. Paleoceanography 20, PA1003. https://doi.org/10.1029/2004PA001071.
Lisiecki, L.E., Raymo, M.E., 2007. Plio–Pleistocene climate evolution; trends and transitions in glacial cycle dynamics. Quat. Sci. Rev. 26, 56–69. https://doi.org/10.1016/j.quascirev.2006.09.005.
Liu, Q., Zhu, R., Pan, Y., Guo, B., 1999. Secular variations in geomagnetic field caused by the fluctuations in the fluid flow in the outer-core. Chin. Sci. Bull. 44 (13), 1214–1218. https://doi.org/10.1007/BF02885969.
Loulergue, L., Schilt, A., Spahni, R., Masson-Delmotte, V., Blunier, T., Lemieux, B., Barnola, J.M., Raynaud, D., Stocker, T.F., Chappellaz, J., 2008. Orbital and millennial-scale features of atmospheric CH4 over the past 800,000 years. Nature 453. https://doi.org/10.1038/nature06950.
Luthi, D., Le Floch, M., Bereiter, B., Blunier, T., Barnola, J.M., Siegenthaler, U., Raynaud, D., Jouzel, J., Fischer, H., Kawamura, K., Stocker, T.F., 2008. High-resolution carbon dioxide concentration record 650,000–800,000 years before present. Nature 453. https://doi.org/10.1038/nature06949.
MacAyeal, D.R., 1993. Binge/purge oscillations of the Laurentide Ice sheet as a cause of the north Atlantic's heinrich events. Paleoceanography 8 (6), 775–784. https://doi.org/10.1029/93PA02200. December 1993.
Mayewski, P.A., Meeker, L.D., Twickler, M.S., Whitlow, S., Yang, Q., Lyons, W.B., Prentice, M., 1997. Major features and forcing of high-latitude norther hemisphere atmospheric circulation using a 110,000 year-long glaciochemical series. J. Geophys. Res. 102 (C12), 345–366. November 30, 1997.
McCracken, K.G., Beer, J., Steinhilber, F., 2014. Evidence for planetary forcing of the cosmic ray intensity and solar activity throughout the past 9400 Years. Sol. Phys. 289 (8), 3207–3229. https://doi.org/10.1007/s11207-014-0510-1.
Meehl, G.A., Arblaster, J.M., Branstator, G., van Loon, H., 2008. A coupled air-sea response mechanism to solar forcing in the Pacific region. J. Clim. 21, 2883–2897. https://doi.org/10.1175/2007JCLI1776.1.
Mörner, N.A., 2013. Planetary beat and solar–terrestrial responses. In: Mörner, N.A., Tattersall, R., Solheim, J.E. (Eds.), Pattern in Solar Variability, Their Planetary Origin and Terrestrial Impacts, Pattern Recognit. In Phys., Special Issue 2013, vol. 1. Copernicus Publications, pp. 107–116. https://doi.org/10.5194/prp-1-107-2013.
Mörner, N.A., Tattersall, R., Solheim, J.E., 2013a. Preface: pattern in solar variability, their planetary origin and terrestrial impacts. In: Mörner, N.A., Tattersall, R., Solheim, J.E. (Eds.), Pattern in Solar Variability, Their Planetary Origin and Terrestrial Impacts, Pattern Recognit. In Phys., Special Issue, vol. 1. Copernicus Publications, pp. 203–204. https://doi.org/10.5194/prp-1-203-2013.
Mörner, N.A., et al., 2013b. General conclusions regarding the planetary–solar–terrestrial interaction. In: Mörner, N.A., Tattersall, R., Solheim, J.E. (Eds.), Pattern in Solar Variability, Their Planetary Origin and Terrestrial Impacts, Pattern Recognit. In Phys., Special Issue, vol. 1. Copernicus Publications, pp. 205–206. https://doi.org/10.5194/prp-1-205-2013.
Neff, U., Burns, S.J., Mangini, A., Mudelsee, M., Fleitmann, D., Matter, A., 2001. Strong coherence between solar variability and the monsoon in Oman between 9 and 6 kyr ago. may 2001 Nature 411, 290–293.
NGRIP Community Members, 2007. Greenland Ice Core Chronology 2005 (GICC05) and 20 Year Means of δ18O Data from NGRIP Back to 60 Ka B2k. Centre for Ice and Climate, University of Copenhagen. http://www.iceandclimate.nbi.ku.dk/data/gicc05_ngrip_60ka_20y_10sep2007.xls.
Ogurtsov, M.G., Nagovitsyn, Y.U.A., Kocharov, G.E., Jungner, H., 2002. Long-period cycles of the sun's activity recorded in direct solar data and proxies. Sol. Phys. 211, 371–394, 2002.
Olsen, L., Hammer, Ø., 2005. A 6-ka climatic cycle during at least the last 50,000 years. Nor. Geol. Unders. Bull. 445, 89–100.
Omerbashich, M., 2006. Galactic-bursts Signatures in Antarctica 10Be Spectra Reveal Cosmogenesis of Climate Switching. https://arxiv.org/pdf/physics/0612185.
Paluś, M., Kurths, J., Schwarz, U., Seehafer, N., Novotná, D., Charvátová, I., 2007. The solar activity cycle is weakly synchronized with the solar inertial motion. Phys. Lett. 365, 421–428. https://doi.org/10.1016/j.physleta.2007.01.039.
Past interglacials working group of PAGES, 2016. Interglacials of the last 800,000 years. Rev. Geophys. 54, 162–219. https://doi.org/10.1002/2015RG000482.
Pestiaux, P., Van der Mersch, Berger, A., Duplessy, J.C., 1988. Paleoclimatic variability at frequencies ranging from 1 cycle per 10 000 years to 1cycle per 1000 years: evidence for nonlinear behaviour of the climate system. Climatic Change 12, 9–37.
Pillans, B., Chappell, J., Naish, T.R., 1998. A review of the Milankovitch climatic beat: template for Plio–Pleistocene sea-level changes and sequence stratigraphy. Sediment. Geol. 122, 5–21.
Rasmussen, S.O., et al., 2014. A stratigraphic framework for abrupt climatic changes during the Last Glacial period based on three synchronized Greenland ice-core records: refining and extending the INTIMATE event stratigraphy. Quat. Sci. Rev. 106, 14–28. https://doi.org/10.1016/j.quascirev.2014.09.007.
Rial, J.A., Pielke Sr., R.A., Beniston, M., Claussen, M., Canadell, J., Cox, P., Held, H., deNoblet-Ducoudré, N., Prinn, R., Reynolds, J.F., Salas, J.D., 2004. Nonlinearities, feedbacks and critical thresholds within the Earth's climate system. Climatic Change 65 (1–2), 11–38.
Rind, D., Lean, J., Lerner, J., Lonergan, P., Leboissitier, A., 2008. Exploring the stratospheric/tropospheric response to solar forcing. J. Geophys. Res. 113 https://doi.org/10.1029/2008JD010114.
Roberts, A.P., Turner, G.M., 2013. Geomagnetic excursions and secular variations. In: Elias, S.A. (Ed.), The Encyclopedia of Quaternary Science, vol. 1. Elsevier, Amsterdam, pp. 705–720.
Rodrìguez-Tovar, F.J., Pardo-Igùzquiza, E., 2003. Strong evidence of high-frequency (sub-Milankovitch) orbital forcing by amplitude modulation ofMilankovitch signals. Earth Planet Sci. Lett. 210, 179–189. https://doi.org/10.1016/S0012-821X(03)00131-6.
Sánchez-Sesma, J., 2015. Multi-millennial-scale solar activity and its influences on continental tropical climate: empirical evidence of recurrentcosmic and terrestrial patterns. Earth Syst. Dynam. Discuss. 6, 1237–1260. https://doi.org/10.5194/esdd-6-1237-2015.
Sánchez-Sesma, J., 2016. Evidence of cosmic recurrent and lagged millennia-scale patterns and consequent forecasts: multi-scale responsesof solar activity (SA) to planetary gravitational forcing (PGF). Earth Syst. Dynam. 7, 583–595. https://doi.org/10.5194/esd-7-583-2016.
Scafetta, N., 2012. Multi-scale harmonic model for solar and climate cyclical variation throughout the Holocene based on Jupiter-Saturn tidalfrequencies plus the 11-year solar dynamo cycle. J. Atmos. Sol. Terr. Phys. https://doi.org/10.1016/j.jastp.2012.02.016.
Scafetta, N., 2014a. The complex planetary synchronization structure of the solar system. In: Mörner, N.A., Tattersall, R., Solheim, J.E. (Eds.), Pattern in Solar Variability, Their Planetary Origin and Terrestrial Impacts. Pattern Recognit. In Phys., Special Issue, vol. 2, pp. 1–19. https://doi.org/10.5194/prp-2-1-2014. Copernicus Publications.
Scafetta, N., 2014b. Discussion on the spectral coherence between planetary, solar and climate oscillations: a reply to some critiques. Astrophys. Space Sci. 354, 275–299. https://doi.org/10.1007/s10509-014-2111-8.
Scafetta, N., Milani, F., Bianchini, A., Ortolani, S., 2016. On the astronomical origin of the Hallstatt oscillation found in radiocarbon and climaterecords throughout the

Holocene. Earth Sci. Rev. 162, 24–43. https://doi.org/10.1016/j.earscirev.2016.09.004.
Schneider, R., Schmitt, J., Köhler, P., Joos, F., Fischer, H., 2013. A reconstruction of atmospheric carbon dioxide and its stable carbon isotopic composition from the penultimate glacial maximum to the last glacial inception. Clim. Past 9, 2507–2523. https://doi.org/10.5194/cp-9-2507-2013.
SeaSolve, 2003. AutoSignalTM Users Guide. Copyright © 2003 by SeaSolve Software Inc, p. 479. All rights reserved.
Shackleton, N.J., 2000. The 100,000-year Ice-Age Cycle Identified and Found to Lag Temperature, Carbon Dioxide, and Orbital Eccentricity. Sci, vol. 289, pp. 1897–1902.
Shang, L., Tian, W., Dhomse, S., Chipperfield, M.P., Liu, Y., Wang, W., 2013. Direct and indirect effects of solar variations on stratospheric ozone and temperature. Chin. Sci. Bull. 58, 3840–3846. https://doi.org/10.1007/s11434-013-5822-2.
Shindell, D.T., Faluvegi, G., Schmidt, G.A., 2020. Influences of solar forcing at ultraviolet and longer wavelengths on climate. J. Geophys. Res. Atmos. https://doi.org/10.1029/2019JD031640 (in press).
Siegenthaler, U., et al., 2005. Stable carbon cycle–climate relationship during the Late Pleistocene. Science 310, 1313–1317.
Solanki, S.K., Usoskin, I.G., Kromer, B., Schussler, M., Beer, J., 2004. Unusual activity of the Sun during recent decades compared to the previous 11,000 years. Nature 431, 28. https://doi.org/10.1038/nature02995.
Steinhilber, F., Abreu, J.A., Beer, J., Brunner, I., Christl, M., Fischer, H., Heikkilä, U., Kubik, P.W., Mann, M., McCracken, K.G., Miller, H., Miyahara, H., Oerter, H., Wilhelms, F., 2012. 9,400 years of cosmic radiation and solar activity from ice cores and tree rings. PNAS, April 109 (16), 5967–5971. www.pnas.org/cgi/doi/10.1073/pnas.1118965109.
Stocker, T.F., Johnsen, S.J., 2003. A minimum thermodynamic model for the bipolar seesaw. Paleoceanography 18 (4), 1087. https://doi.org/10.1029/2003PA000920.
Sun, B., Bradley, R.S., 2002. Solar influences on cosmic rays and cloud formation: a reassessment. J. Geophys. Res. 107.
Sun, J., Huang, X., 2006. Half-precessional cycles recorded in Chinese loess: response to low-latitude insolation forcing during the last interglaciation. Quat. Sci. Rev. 25 (9–10), 1065–1072. https://doi.org/10.1016/j.quascirev.2005.08.004.
Svensmark, H., Friis-Christensen, E., 1997. Variation of cosmic ray flux and global cloud coverage - a missing link in solar-climate relationships. J. Atmos. Sol. Terr. Phys. 59 (11), 1225–1232.
Tarnocai, C., Canadell, J.G., Schuur, E.A.G., Kuhry, P., Mazhitova, G., Zimov, S., 2009. Soil organic carbon pools in the northern circumpolar permafrost region. Global Biogeochem. Cycles 23, GB2023. https://doi.org/10.1029/2008GB003327.
Turney, C.S.M., Kershaw, A.P., Clemens, S.C., Branch, N., Moss, P.T., Fifield, L.K., 2004. Millennial and orbital variations of El Nino/Southern Oscillation and high-latitude climate in the last glacial period. Nature 428, 18. https://doi.org/10.1038/nature02386. March 2004.
Tziperman, E., Raymo, M.E., Huybers, P.J., Wunsch, C., 2006. Consequences of pacing the Pleistocene 100 kyr ice ages by nonlinear phase locking to Milankovitch forcing. Paleoceanography 21 (PA4206), 1–11. https://doi.org/10.1029/2005PA001241.
Usoskin, I.G., Gallet, Y., Lopes, F., Kovaltsov, G.A., Hulot, G., 2016. Solar activity during the Holocene: the Hallstatt cycle and its consequence for grand minima and maxima. Astron. Astrophys. 587, A150. https://doi.org/10.1051/0004-6361/201527295.
Usoskin, I.G., 2017. A history of solar activity over millennia. Living Rev. Sol. Phys. 14, 3. https://doi.org/10.1007/s41116-017-0006-9.
Vautard, R., Ghil, M., 1989. Singular spectrum analysis in nonlinear dynamics, with applications to paleoclimatic time series. Physica D 35, 395–424 (North-Holland, Amsterdam).
Viaggi, P., 2018. δ18O and SST signal decomposition and dynamic of the Pliocene-Pleistocene climate system: new insights on orbital nonlinear behavior vs.long-term trend, 2018 Prog. in Earth and Planet. Sci. 5, 81. https://doi.org/10.1186/s40645-018-0236-z, 7 December 2018.
Vieira, L.E.A., Solanki, S.K., Krivova, N.A., Usoskin, I., 2011. Evolution of the solar irradiance during the Holocene. Astron. Astrophys. 531, 2011. https://doi.org/10.1051/0004-6361/201015843. March 29.
Walker, M., Gibbard, P., Head, M.J., Berkelhammer, M., Björck, S., Cheng, H., Cwynar, L. C., Fisher, D., Gkinis, V., Long, A., Lowe, J., Newnham, R., Rasmussen, S.O., Weiss, H., 2019. Formal subdivision of the Holocene series/epoch: a summary. J. Geol. Soc. India 93 (Feb), 135–141. https://doi.org/10.1007/s12594-019-1141-9.
Willeit, M., Ganopolski, A., 2018. The importance of snow albedo for ice sheet evolution over the last glacial cycle. Clim. Past 14, 697–707. https://doi.org/10.5194/cp-14-697-2018.
Wu, H., Zhang, S., Feng, Q., Jiang, G., Li, H., Yang, T., 2012. Milankovitch and sub-Milankovitch cycles of the early Triassic Daye Formation, South China and their geochronological and paleoclimatic implications. Gondwana Res. 22, 748–759. https://doi.org/10.1016/j.gr.2011.12.003.
Wu, C.J., Usoskin, I.G., Krivova, N., Kovaltsov, G.A., Baroni, M., Bard, E., Solanki, S.K., 2018a. Solar activity over nine millennia: a consistent multi-proxy reconstruction. Astron. Astrophys. 615, A93. https://doi.org/10.1051/0004-6361/201731892.
Wu, C.J., Krivova, N.A., Solanki, S.K., Usoskin, I.G., 2018b. Solar total and spectral irradiance reconstruction over the last 9000 years. Astron. Astrophys. 620, A120. https://doi.org/10.1051/0004-6361/201832956.
Wunsch, C., 2004. Quantitative estimate of the Milankovitch-forced contribution to observed Quaternary climate change. Quat. Sci. Rev. 23, 1001–1012. https://doi.org/10.1016/j.quascirev.2004.02.014.
Xapsos, M.A., Burke, E.A., 2009. Evidence of 6000-year periodicity in reconstructed sunspot numbers. Sol. Phys. 257, 363–369. https://doi.org/10.1007/s11207-009-9380-3.
Yndestad, H., Solheim, J.E., 2016. The influence of solar system oscillation on the variability of the total solar irradiance. N. Astron. 51 https://doi.org/10.1016/j.newast.2016.08.020. August 2016.
Zhao, X.H., Feng, X.S., 2015. Correlation between solar activity and the local temperature of Antarctica during the past 11,000 years. J. Atmos. Sol. Terr. Phys. 122, 26–33. https://doi.org/10.1016/j.jastp.2014.11.004.
Zharkova, V.V., Shepherd, S.J., Zharkov, S.I., Popova, E., 2019. Oscillations of the baseline of solar magnetic field and solar irradiance on amillennial timescale. Sci. Rep. 9, 9197. https://doi.org/10.1038/s41598-019-45584-3.